LANGMUIR Article
Cite This: Langmuir XXXX, XXX, XXX−XXX
pubs.acs.org/Langmuir

Direct Measurement of Water Permeation in Submerged Alkyl Thiol Self-Assembled Monolayers on Gold Surfaces Revealed by Neutron Reflectometry

Whitney A. Fies,[†] Jason W. Dugger,[‡] Jeffrey E. Dick,[§] Logan M. Wilder,[†] Katie L. Browning,[∥] Mathieu Doucet,[⊥] James F. Browning,[⊥] and Lauren J. Webb*[,†]

[†]Department of Chemistry and Texas Materials Institute, The University of Texas at Austin, 2506 Speedway STOP A5300, Austin, Texas 78712, United States

[‡]Center for Nanophase Materials Sciences, [∥]Materials Science and Technology Division, and [⊥]Neutron Scattering Division, Oak Ridge National Laboratory, Oak Ridge, Tennessee 37831, United States

[§]Department of Chemistry, The University of North Carolina at Chapel Hill, Chapel Hill, North Carolina 27599, United States

Supporting Information

ABSTRACT: Self-assembled monolayers (SAMs) of alkyl thiols are frequently used to chemically functionalize gold surfaces for applications throughout materials chemistry, electrochemistry, and biotechnology. Despite this, a detailed understanding of the structure of the SAM−water interface generated from both formation and use of the SAM in an aqueous environment is elusive, and analytical measurements of the structure and chemistry of the SAM−water interface are an ongoing experimental challenge. To address this, we used neutron reflectometry (NR) to measure water association with both hydrophobic and hydrophilic SAMs under both wet and dry conditions. SAMs used for this study were made from hydrophobic decanethiol mixed with hydrophilic 11-azido-1-undecanethiol with compositions of 0−100% of the azide-terminated thiol. All SAMs were formed by conventional solution incubation of a Au substrate immersed in ethanol. Each SAM was characterized by grazing incidence angle reflection−absorption Fourier transfer infrared spectroscopy, contact angle goniometry, and electrochemical methods to confirm it was a completely formed monolayer with evidence of extensive crystalline-like domains. NR measured significant absorption of water into each SAM, ranging from 1.6 to 5.7 water molecules per alkyl thiol, when SAMs were immersed in water. Water infiltration was independent of SAM composition and terminal group hydrophilicity. These results demonstrate that water accesses defects, fluid regions, and heterogeneous domains inherent to even well-formed SAMs.

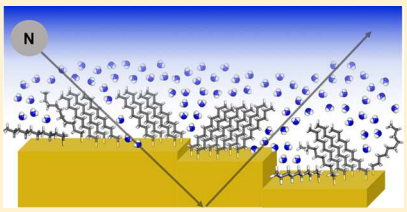

INTRODUCTION

Self-assembled monolayers (SAMs) are spontaneously ordered molecular assemblies chemisorbed to an ordered surface and are used in a variety of applications ranging from custom microelectronics to templates that mimic biological membranes. SAMs based on alkane thiols on Au surfaces are attractive materials for these purposes because they are easy to prepare, they allow for customizable surface chemistry, and they provide a physical barrier between a conducting surface and its environment. Because of these advantages, SAMs are used ubiquitously throughout chemistry, biology, materials science, and beyond since they were first demonstrated in 1983 by Nuzzo and Allara.[1] Modulating SAM thickness and functionality is accomplished by simply choosing the chain length and chemical functionality of the alkane thiol in order to tailor the surface to the desired application. The resulting SAMs are stable against decomposition in ambient conditions for days, under vacuum, and in a range of solvents including water, tetrahydrofuran, dimethylformamide, toluene, and ethanol.[2]

The structure of SAMs on Au is defined by three components: (1) a Au−sulfur bond that anchors each thiol molecule; (2) an alkyl chain that provides the driving force for self-assembly by maximizing van der Waals interactions between neighboring molecules; and (3) a terminating functional group that defines the chemical reactivity of the SAM surface. A slightly simplified view of SAM formation begins in solution as the thiols displace solvent molecules from the Au surface and sulfur binds to Au. Initially, the alkyl bodies lie parallel to the Au surface in different configurations, all of which are considered "lying-down" phases. As more thiols bind to the Au surface, they transition to a more upright phase because of intermolecular crowding. This occurs as the alkyl bodies spontaneously align themselves with one another to maximize van der Waals intermolecular forces. The "standing-up" phase grows denser over time, adopting crystalline-like, high-coverage, close-packed domains.[3,4] The alkyl portion of the thiol that comprises the bulk of the SAM has been demonstrated with many functional groups such as alkanes, alkenes, esters, phenyl rings, and others,[5,6] but saturated alkyl chains of varying lengths have been examined to the greatest

Received: February 23, 2019
Published: March 28, 2019

DOI: 10.1021/acs.langmuir.9b00541
Langmuir XXXX, XXX, XXX−XXX

degree. On well-characterized Au(111) surfaces, alkyl thiols align into domains with a $(\sqrt{3} \times \sqrt{3})R30°$ overlayer structure and a sulfur atomic spacing of 5 Å.[7,8] However, other Au crystal faces induce alternative sulfur atomic spacing and organization. The terminal group of the thiol defines the hydrophilicity of a SAM surface and can be used as a precursor for further functionalization. For example, azide-terminated thiols have been used as precursors for Huisgen cycloaddition reactions, which bind larger molecular structures to Au.[9,10] SAMs can be successfully made using vastly different functional groups without significantly disrupting the formation of close-packed domains, but bulky or strong hydrogen bonding terminal groups affect the self-assembly process and the overall structure.[3]

The highly ordered "standing-up" domains on Au(111) are the hallmark depiction of the SAM structure and are universally used to represent their structure in cartoon schematics and even computational simulations. However, the mesoscopic structure of the SAM is much more complex and is not solely a conglomerate of ordered crystal domains. In addition to different types of ordered domains imposed by other Au faces and grain boundaries, the overall SAM structure is impacted by interdomain boundaries, adatoms, vacancy islands, pinholes, Au step edges, and amorphous SAM regions. In particular, polycrystalline Au, which is the most common substrate for preparing SAMs, produces more inhomogeneities and defects into SAMs than single-crystal Au. These defects are exacerbated with increased microscopic surface roughness. Au deposited on Si is a common substrate used to form SAMs because of its low cost and ease of fabrication, but the surface is rougher than Au deposited on mica or crystalline Au and the resulting SAM will inherently have more defects. Furthermore, SAMs themselves are not truly crystalline at room temperature but more akin to the gel phase of a liquid crystal; the terminal ends of SAMs are thermally mobile and an increase in the number of gauche conformers has been observed toward the terminal group of a SAM, even in highly ordered regions.[4,11]

The prevalence of SAMs throughout chemistry, materials science, and biotechnology in recent decades has increased because they are versatile and easy to prepare. As a result, it has become common for researchers to forgo thorough SAM characterization when they are used as a platform for other experiments. It is now quite common for published reports to assume that the close-packed crystalline domains represent the entirety of the SAM surface or that the presence of assumed defects does not affect the experimental results without characterization. Essentially, SAMs have been expected to be a thin, uniform, physical barrier between Au and its environment. Yet, SAM defects can dramatically change the properties of a SAM at a molecular level and potentially change the interactions between the SAM and its environment. For instance, small ions have been reported to travel through SAMs and passivate Au,[12−16] and even larger ions, like ruthenium complexes, have permeated SAMs in regions known to be amorphous.[17] This directly contradicts the assumption that SAMs are a uniform layer that blocks the underlying Au surface.

The extent and origin of structural defects in SAMs have historically been investigated with a variety of techniques including electrochemistry,[12,14,18,19] chemical etching,[12,20] and scanning tunneling microscopy (STM).[21,22] Although it is well-known that SAMs contain defects and that certain ions can penetrate their structure, there is little information available on how solvents, particularly water, interact with SAMs at disordered (gel-like) regions and defect sites. This represents a gap in understanding the nature of the SAM layer. Information on the water−SAM interface is particularly important because SAMs are used in an assortment of aqueous experiments because they are stable in water. For example, they are especially valuable for electrochemistry, where they are used as a barrier between the electrolyte or redox species and the electrode[5] or as a way to bind redox species at the electrode surface.[23−25] Their stability in a variety of aqueous conditions also makes them an excellent experimental platform for investigating biological systems, as demonstrated by their extensive use in bioconjugating proteins to surfaces[25−28] and as models for studying biological membranes.[29] Furthermore, the hydrophobicity of methyl-terminated SAMs has been exploited to create coatings to block corrosion.[15] In all these applications, discerning how water interacts with SAMs is important for developing a complete understanding of the interaction between the surface and the environment.

Since their discovery, SAMs have been extensively characterized with a variety of techniques, such as STM, electron diffraction, and grazing incidence angle reflection−absorption surface Fourier transform infrared spectroscopy (GRAS−FTIR), which have all been used to determine the packing density and formation of the overlayer structure.[7,8,18,22,30−32] X-ray photoelectron spectroscopy (XPS) has been used for determining SAM composition, especially in mixed SAMs,[33,34] and for distinguishing between "lying-down" and "standing-up" phases.[35,36] In more recent years, computational modeling of SAMs or SAM-like surfaces exposed to a variety of conditions, including water, has become more sophisticated and reliable.[37,38] Experimental approaches to quantifying water−SAM interactions have largely relied on contact angle goniometry, which has successfully measured SAM wettability as a function of pH and SAM terminal group.[33,39,40] However, the macroscopic hydrophilicity of a surface measured by water contact angles offers no information on the intermolecular interactions at the water−SAM interfaces that occur in aqueous systems.

The work described here focuses on characterizing the presence and structure of water near or within the SAM layer using neutron reflectometry (NR) in combination with other analytical techniques. NR is a powerful tool for investigating complex, laminar systems and for quantitatively characterizing water within that system. NR is nondestructive and has been extensively used to measure soft matter, such as probing solvent effects on poly(*N*-isopropylacrylamide) conformational changes,[41] the structure and orientation of amelogenin on surfaces,[42] and to quantify hydration in biological membranes as a function of humidity.[43] NR is capable of differentiating the thickness and composition between layers with subnanometer resolution, providing information on the penetration of molecules into the multilamellar stack. In addition, neutrons scatter uniquely with each isotope, allowing for experimental manipulation known as "contrasting" in which hydrogen is replaced with deuterium, highlighting components of the system that contain hydrogen, including water associated with a particular layer at the interface. Additionally, contrasting can highlight any water associated with a particular layer when the system is exposed to wet or humid environments.

In this investigation, we characterized SAMs composed of alkyl chains of 10 and 11 carbons in length ranging from 100% methyl-terminated thiols to 100% azide-terminated thiols, with

DOI: 10.1021/acs.langmuir.9b00541
Langmuir XXXX, XXX, XXX−XXX

25% increments of mixed thiol compositions, on Au surfaces. The structure and integrity of SAMs were evaluated with GRAS−FTIR, contact angle goniometry, and cyclic voltammetry (CV). Macroscopically, azide-terminated SAMs were hydrophilic, methyl-terminated SAMs were hydrophobic, and mixed SAMs were intermediate between these two extremes as hydrophilicity increased linearly with increasing azide surface concentration. We quantified water infiltration into mixed SAMs varying from 25%/75% azide-/methyl-terminated thiols to 100% azide-terminated thiols. The NR of these SAMs in ambient air and when entirely immersed in contrasting aqueous conditions were measured to calculate water uptake into the SAM layer. Regardless of the terminal functional group, we found water molecules to be intercalated into the SAM and in contact with exposed Au when immersed in water. As we demonstrate below, our SAMs were well formed and were comparable to previously reported SAMs made by incubating Au surfaces in the thiol-containing solution. Using NR, we discovered that the conventional defects and disordered regions found in these SAMs allowed for the inclusion of water within the SAM layer when the SAM was fully immersed in aqueous solutions.

EXPERIMENTAL SECTION

Surface Functionalization. Substrates for FTIR, CV, and contact angle goniometry were generated from 500 μm thick, 100 mm diameter n-type Si(111) wafers (University Wafer) polished on one side and sealed in N_2(g). The sealed wafers were opened and stored in dry N_2(g) atmosphere inside a glovebox. Wafers were transferred to an electron beam deposition chamber (Cooke Vacuum Products) in a class 100/1000 cleanroom. The surfaces were covered in 5−10 nm of Cr, followed by 200 nm of Au (99.95% pure, Kurt J. Lesker) at a pressure of no greater than 10^{-5} Torr and a substrate temperature of 110 ± 10 °C. After the deposition of Au, the wafers were attached to the Si wafer tape (ICROS TAPE) and cut with a programmable Disco 321 wafer dicing saw into pieces of approximately 1 cm^2. The wafers were then kept on the tape and stored in deionized water until cleaned. Each substrate was sonicated for 10 min in acetone, followed by 10 min in ethanol, and dried under a stream of N_2(g) to remove any tape residue or contaminates from the dicing saw. Cut, cleaned wafers were covered and stored in air prior to use. Immediately before SAM formation, wafers were immersed for 1−3 min in piranha solution (1:3 30% hydrogen peroxide/concentrated sulfuric acid; **Caution**: *explosive in the presence of organic contaminants*) and then rinsed in ultrapure water (18.2 MΩ cm^{-1}, Barnstead NANOpure Diamond Life Science UV/UF) and anhydrous ethanol. The samples were dried under a stream of N_2(g) and subsequently annealed with a hydrogen flame for 5 min. Once cooled to room temperature, substrates were immediately transferred to the thiol solution.

Substrates for neutron reflectivity were n-type Si(111). They were 50 mm diameter, 5 mm thick, and polished on one side (purchased from both University Wafer and El-Cat). Substrates were immersed in piranha solution for 10 min, rinsed in high-purity water, and dried under a stream of N_2(g) before coating. Samples used for this work were made from wafers coated with Cr and Au in three different batches. The first batch was coated in an electron beam deposition chamber (Cooke Vacuum Products) in a class 100/1000 cleanroom with a Cr thickness of 1−8 nm and a Au thickness of 20 nm. The second batch was fabricated at the National Institute for Standards and Technology (NIST) Center for Nanoscale Science and Technology with a Cr thickness of 4 nm and a Au thickness of 42 nm. The third was made by physical vapor deposition using a radio frequency source in an in-house chamber with dual guns at Oak Ridge National Laboratory (ORNL), with film thicknesses of 5 nm Cr and 60 nm Au estimated by quartz crystal microbalance (QCM).

Thiol solutions (1 mM) were made by diluting the desired thiol in anhydrous ethanol. For the SAMs, 11-bromo-1-undecanethiol (BrUDT, 99% purity, Sigma-Aldrich) was mixed with either hydrogenated (DT, 96%, Sigma-Aldrich) or deuterated (D21, 98 atom % D, C/D/N isotopes) decanethiol to desired concentrations, keeping the total thiol concentration at 1 mM. The Au-coated substrates were immersed in the 1 mM thiol solutions for 24 h at room temperature. Samples were rinsed in high-purity water, followed by anhydrous ethanol, and dried under a stream of N_2(g). Subsequently, the bromine on the bromine-terminated or partially bromine-terminated SAMs was replaced with azide to create 11-azido-1-undecanethiolated (AzUDT) Au by immersing the SAMs in a saturated solution of sodium azide in *N*,*N*-dimethylformamide (DMF) and incubated for 48 h in the dark at room temperature. After reacting with azide, samples were rinsed in high-purity water and then in DMF consecutively two times. Samples were then rinsed in ethanol and dried under a stream of N_2(g). 11-azido-1-undecanethiol was synthesized to create a 100% azide-terminated SAM without NaN_3 contamination (100AzUDT-p). Thiol synthesis was accomplished with previously published methods.[44] $MgSO_4$, NaN_3, thioacetic acid, dry methanol, acetyl chloride, diethyl ether, azobisisobutyronitrile, and 11-bromo-1-undecene were purchased from MilliporeSigma. Toluene, hexane, dimethylformamide, dichloromethane and sodium chloride were purchased from Fisher Scientific. 100AzUDT-p was created by incubating Au surfaces in a 1 mM ethanolic solution in the dark at room temperature for 24 h. The two thiolate structures that created the final SAM compositions are depicted in Figure 1.

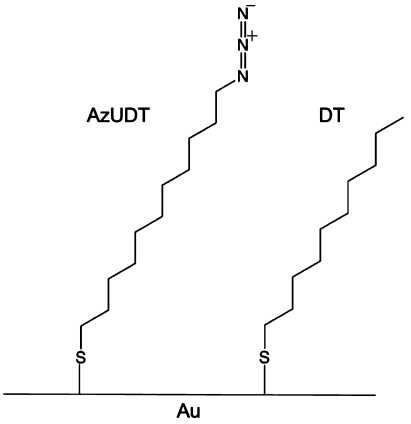

Figure 1. Chemical structures of the two SAM components used for this study.

Grazing Incidence Angle Reflection−Absorption Surface Fourier Transform Infrared Spectroscopy. A Bruker Vertex 70 FTIR spectrometer equipped with an A518/Q Horizontal Reflection (Bruker) accessory was used to obtain all FTIR spectra. The samples were scanned at a grazing angle of 80° with respect to the surface normal with p-polarized light. The sample compartment was continuously purged with N_2(g), and samples were exchanged with a home-built externally controlled sample handling tool, keeping the sample chamber from atmospheric exposure. The compartment was purged for 1 h prior to measurement, effectively reducing background noise from H_2O and CO_2. Depending on the wavenumber range of the spectrum, two different detectors were used: (1) a mercury cadmium telluride (MCT) detector collected scans between 400 and 4000 cm^{-1} at a resolution of 4 cm^{-1} and (2) an indium antimonide (InSb) detector collected scans between 1870 and 4000 cm^{-1} at a resolution of 4 cm^{-1}. All sample spectra were background-subtracted using a clean, bare Au substrate and baseline-corrected with a polynomial function. Peak values were computed using Wavemetric's MultiPeakFit package in Igor Pro by applying Gaussian fits to raw data.

Electrochemistry. CV was performed with a potentiostat (600E series electrochemical analyzer, CH Instruments) using an Ag/AgCl reference electrode (CH Instruments) and a Pt wire counter electrode

DOI: 10.1021/acs.langmuir.9b00541
Langmuir XXXX, XXX, XXX−XXX

(CH Instruments). A home-built Teflon electrochemical cell was used for all electrochemical measurements. In the electrochemical cell, Au surfaces were used as the active working electrode. A connection was made to these surfaces by a copper tape that was adhered to Au with Ag paint (PELCO). A 5 mm o-ring was used to seal the Teflon cell to the Au surface, and care was taken to ensure the copper tape did not have access to the solution. The Au surfaces were sealed to the Teflon cell by a plastic plate with four screws.

To determine SAM coverage, each SAM composition was cycled between 0 and −1.5 V (vs Ag/AgCl) at 100 mV s^{-1}, stripping the thiols from the Au surface. Surfaces were stripped in a solution of 100 mM NaOH that had been bubbled with Ar gas for at least 15 min. At least four replicates of each SAM composition were analyzed. We assumed that the stoichiometric number of electrons involved in the reduction of the thiol was one.[21] The real surface area of Au was measured with two methods, which are described in detail in the Supporting Information. The surface area used for SAM coverage calculations was determined by obtaining the charge under a AuO reduction peak of Au deposited on Ti (Figure S3). This value was 0.43 ± 0.05 cm^2, corresponding to a roughness factor of 1.2. Using Faraday's law, the integrated charge under the cathodic peak is directly proportional to thiol coverage. The integrated charge was converted to a surface coverage (SC) in units of molecules cm^{-2} using eq 1

$$\mathrm{SC} = QN_\mathrm{A}/(nFS_\mathrm{A}) \tag{1}$$

where N_A is Avogadro's number, Q is the integrated charge, n is the stoichiometric number of electrons (1), F is Faraday's constant, and S_A is the surface area of Au.

The integrity of each SAM was judged electrochemically by measuring the ability of each SAM to block charge transfer from the outer-sphere redox reaction, $Fe(CN)_6^{3-}/Fe(CN)_6^{4-}$, to Au. Using the same home-built electrochemical cell described above, 1 mM potassium ferricyanide (Sigma-Aldrich) in 1 M KCl was cycled from 0.5 to −0.2 V (vs Ag/AgCl) at 100 mV/s on at least three replicates of each SAM composition in addition to clean bare Au surfaces. A grounding bracelet was worn to safeguard against static discharge. The ability of the SAM to block charge transfer to the Au surface was qualitatively determined by the disappearance of peak potentials of the redox couple.

Contact Angle Goniometry. Water contact angle measurements were made with a FTA200 contact angle goniometer in a class 100/1000 cleanroom. Deionized water was used, and the water droplet size was kept consistent between measurements using an automated syringe dispenser. At least two measurements were made on each sample, and there were three replicates for each surface type. Error reported is the standard deviation of at least six measurements. The contact angle value was reported by the instrument's FTA32 software using an auto nonspherical fit to the liquid−vapor interface.

Neutron Reflectometry. Because of their wavelike nature, neutrons can be reflected and/or refracted at an interface separating materials of different indices of refraction following Snell's law. In a NR measurement, the extent of specularly reflected neutrons from the surface of a thin film is measured as a function of the wave vector transfer, Q, perpendicular to the surface (eq 2)

$$Q = (4\pi \sin\theta)/\lambda \tag{2}$$

where θ is the angle of incidence and λ is the wavelength of the neutron beam. Figure 2 illustrates the neutron beam path through a sample cross section in which Q is described as the difference between the initial, $k_{i,z}$, and final, $k_{f,z}$, wave vectors of the incoming and reflected beam. The resulting reflectivity is dependent on each layer's thickness, scattering length density (SLD), and interfacial roughness, measured perpendicular to the substrate surface as the incident beam of neutrons is either reflected or refracted by interfaces comprising each thin layer on a substrate. SLD is described by eq 3

$$\mathrm{SLD} = \frac{\sum b_i}{V_\mathrm{m}} \tag{3}$$

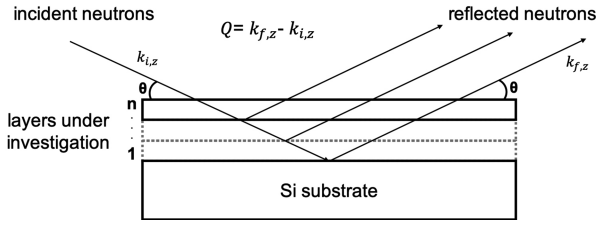

Figure 2. Depiction of a NR experiment on a multilaminar thin-film sample.

where Σb_i is the sum of the neutron scattering lengths of all atoms in a molecule and V_m is the molecular volume. Measured reflectivity is plotted as a function of Q, and a graph of reflectivity versus Q, called a reflectivity profile, is interpreted by applying either the Abeles matrix method or Parratt's formalism[45] for reflectivity to determine the thickness, SLD, and roughness of each layer above the substrate surface. The resulting calculated model is rated on goodness of fit by a standard χ^2 test, which quantifies how well the model and the data correlate with a least squares analysis.

NR measurements were performed at ORNL's Spallation Neutron Source on the Liquids Reflectometer, beamline BL-4B. Q ranges spanned 0.008−0.238 $Å^{-1}$ by changing both the angle of incidence (0.60°−2.71°) and the wavelength range of the incident beam (2.5−16.75 Å) in seven intervals. Neutrons were detected by time-of-flight with a two-dimensional position sensitive ^{3}He detector.

The reflectivity of each sample was first measured in ambient air, and then each sample was scanned while immersed in water. Two different aqueous solutions were used for each sample: D_2O and 70/30 v/v D_2O/H_2O. The mixture of D_2O/H_2O was chosen because the SLD of this mixture ratio was approximately the same value as Au, highlighting the SAM layer with a distinct SLD value. Wet runs were completed in a liquid cell, which sealed the SAM surface in a liquid environment with a Viton o-ring pressed between the sample and a 10 mm thick Si wafer cell cover. The sample and 10 mm Si wafer were bolted together using aluminum (sample side) and stainless steel (topside) plates. Once sealed, the chamber was filled with approximately 2 mL of liquid through two, 1 mm diameter holes milled through the 10 mm thick Si wafer. Wet runs differed from air runs because the liquid cell necessitated an inverted sample geometry, requiring the beam to enter and exit the supporting Si substrate of the sample. For 25AzUDT, we later determined that the 70/30 D_2O/H_2O data were likely corrupted by an air bubble within the liquid/solid cell (refer to the Supporting Information). This sample was also measured in H_2O, and so, the H_2O data were used in place of the 70/30 D_2O/H_2O data for the final calculations and conclusions.

Reflectivity data were analyzed using the Motofit analysis package within Igor (Wavemetrics) and with ORNL's Web Interface (Webi).[46,47] Motofit uses the Abeles matrix method on a system with n number of slabs to fit a model to reflectivity data, where each slab is described by a thickness, SLD, and interfacial roughness. A highly iterative process of applying least squares minimization, genetic optimization, and Monte Carlo error analysis was used to fit the data by minimizing the χ^2 distribution value and maintaining physical relevance of the model to the system by correlating possible results to other analytical techniques. In contrast, Webi runs on the REFL1D scripts provided by the National Institute of Standards and Technology (NIST).[48] This is also an iterative process using the Nelder−Mead and DREAM algorithms to fit data, minimizing the χ^2 distribution value, and comparing the results to other analytical techniques to judge physical relevance. SLD values for the Cr and Au layers were obtained by allowing the model to vary up to 10% of the published bulk values (Cr: 3.03 × 10^{-6} $Å^{-2}$, Au: 4.67 × 10^{-6} $Å^{-2}$) to account for defects and low density resulting from the deposition process, and the SLD of Si was held constant to the published value (2.07 × 10^{-6} $Å^{-2}$).[49] The SLD of the native oxide layer on Si varied from sample to sample, but values were correlated to the individual wafer's vendor and batch. Data sets were simultaneously fit if measured consecutively in the same geometry to ensure confidence in

DOI: 10.1021/acs.langmuir.9b00541
Langmuir XXXX, XXX, XXX−XXX

the thickness, SLD, and roughness values in each of the inorganic layers. Parameters associated with the inorganic layers (Si, SiO_x, Cr, Au) were allowed to vary up to 10% between data sets that were not simultaneously fit to grant for systematic variation that occurs between taking measurements in varying geometries. Au absorption (imaginary SLD of 0.0162×10^{-6} Å^{-2}) was apparent if Au thickness was >50 nm and the sample mediums' SLDs continuously increased (e.g., Si < Au < D_2O), resulting in slightly nonlinear reflectivity before the critical wave transfer vector, Q_c. An example of observed Au absorption is shown in Figure S7. All other chemicals' SLD values were calculated using their atomic neutron scattering lengths tabulated by NIST,[50] their molar masses, and their respective densities (see eq 3). SLDs of bulk D_2O (6.36×10^{-6} Å^{-2}) and 70/30 v/v D_2O/H_2O (4.27×10^{-6} Å^{-2}) were initially allowed to vary in the models by as much as ±10% of their theoretical values to account for any impurities or, in the case of 70/30 v/v D_2O/H_2O, volumetric measurement errors.

Theoretical SLD values for SAMs represent a completely close-packed, full monolayer with a ~30° title angle. Detailed calculations of the SAM SLDs are supplied in the Supporting Information. Because the composition of the SAM layer changed based on its environment and coverage, the model parameters for the SAM were allowed to float until all remaining layers were defined. SAM thicknesses were constrained to the most physically plausible height ranges of the SAM. The maximum height assumed a height of 1.4 Å per methylene group and oriented perpendicular to the surface. The minimum height was set to the value of the respective SAM assuming a height of 1.1 Å per methylene group and a tilt angle of 40° with respect to the surface normal. Our reported values for the SAM layers have the lowest χ^2 value within reasonable physical limits of thickness and density.

The number of water molecules per alkyl thiol in the SAM layer was determined by eq 4

$$n = \left(S_{SW} \times V_m - \sum b_S\right) / \sum b_W \quad (4)$$

where n is the number of water molecules per thiol, S_{SW} is the SLD of the SAM layer immersed in water, V_m is the experimental molecular volume of the SAM, Σb_S is the scattering length of the SAM molecule, and Σb_W is the scattering length of water or heavy water. In this way, NR was able to directly measure the amount of water associated with the SAM layer.

RESULTS AND DISCUSSION

It was essential to first understand the structure of the SAMs in order to develop a physical representation of the NR results. On the basis of the literature precedent, the procedure that we followed for fabricating alkane thiol monolayers should have resulted in an ordered SAM with high SC. To ensure this, our monolayers were analyzed with four common techniques used to evaluate SAM coverage and structure: water contact angle goniometry, GRAS–FTIR, cathodic stripping voltammetry, and heterogeneous electron transfer. Each of these techniques provides unique information about the structure and chemistry of the SAM with accompanying advantages and disadvantages that are addressed individually in subsequent sections. Currently, however, there are still open questions about the molecular-level structure of SAMs that this collection of techniques is incapable of addressing directly. In this report, we demonstrate that NR provides critical orthogonal information to these standard techniques.

Five SAM compositions that varied in terminal group functionality were prepared for characterization (abbreviations used throughout this work are given in parenthesis): 100% 11-azido-1-undecanethiol (100AzUDT); 75% 11-azido-1-undecanethiol, 25% decanethiol (75AzUDT); 50% 11-azido-1-undecanethiol, 50% decanethiol (50AzUDT); 25% 11-azido-1-undecanethiol, 75% decanethiol (25AzUDT); and 100% decanethiol (100DT). We have previously shown that mixed SAMs with precise surface compositions of DT and AzUDT can be made with solution concentrations of the same thiol ratio desired on the surface.[51] In the case of the neutron experiments, deuterated d_{21}-decanethiol was used in place of decanethiol because its SLD (5.99×10^{-6} Å^{-2}, liquid density) is significantly greater than that of hydrogenated decanethiol (-0.26×10^{-6} Å^{-2}, liquid density), creating a greater degree of contrast between the system components (SAM, bulk Au, and air or water). All SAM labels are for hydrogenated SAMs unless otherwise noted by "(D21)".

Contact Angle Goniometry. Water contact angle goniometry is a straightforward way to determine the macroscopic hydrophobicity/hydrophilicity of a surface and has long been used to assess SAM quality. To confirm that the samples prepared for this study exhibited the expected macroscopic properties of well-formed SAMs, the advancing contact angles of water on all of our SAM compositions were measured (Figure 3). An advancing contact angle of water that

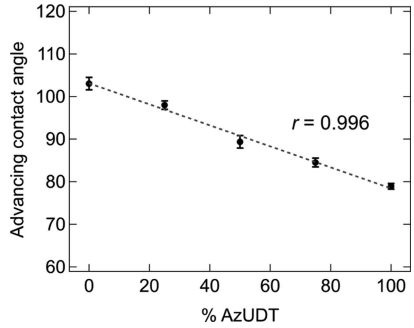

Figure 3. Advancing water contact angle on surfaces composed of increasing AzUDT/DT composition in the mixed SAM monolayer. 0% AzUDT is a 100DT surface. Errors are plotted as the standard deviations of at least six droplets on a total of at least three samples.

is greater than 90° is indicative of a hydrophobic surface, whereas one of less than 90° is hydrophilic. The advancing contact angle of a clean bare Au surface prior to SAM formation was clearly hydrophilic (49.6 ± 1.5°) and was within the range of angles of Au surfaces reported elsewhere (40°–60°).[52] For all SAM compositions, the advancing contact angle of water was dramatically different from that of bare Au, ranging from 79° to 103° (Figure 3), implying that the SAM dictated the surface chemistry. Furthermore, the SAMs followed a distinct linear trend of increasing hydrophilicity as the concentration of AzUDT was increased within the mixed monolayer. These observed macroscopic surface properties are consistent with well-formed SAMs.[39,53,54] Additionally, the 100DT contact angle (103.0 ± 1.5°) was similar to what has been reported for longer aliphatic chains (103°–116°).[21,52,53] Collectively, the contact angles demonstrate that these SAMs are well described by the literature precedent. However, more information is needed to determine the overall structure and quality of the SAM. Although contact angle data are valuable for determining the macroscopic chemical properties of monolayer terminal groups, they do not provide information on the microscopic properties of SAMs because water contact angles do not differ significantly with changes in crystallinity or microscopic inhomogeneity of SAMs.[39] Furthermore, they do not provide information about interactions at the molecular

DOI: 10.1021/acs.langmuir.9b00541
Langmuir XXXX, XXX, XXX–XXX

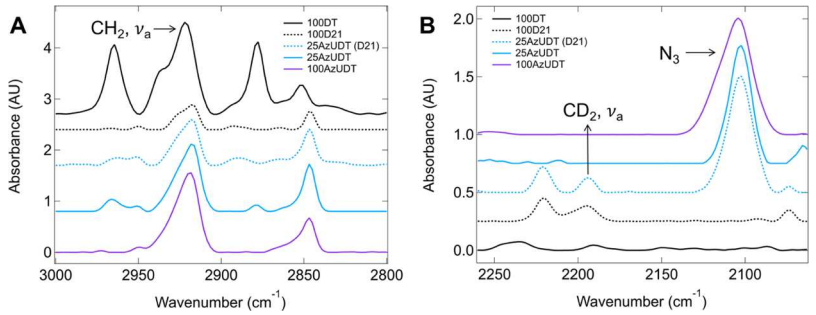

Figure 4. GRAS–FTIR spectra of representative SAM samples. Solid lines are spectra of hydrogenated SAMs, and dotted lines are spectra of SAMs with D21 in replacement of DT. 100% decanethiol surfaces are shown in black; 25AzUDT surfaces are shown in blue; 100AzUDT surfaces are shown in purple. (A) Methyl and methylene stretching region. The ν_a mode for CH_2 is highlighted. (B) Deuterated methyl and methylene stretching region and azide stretching mode. The azide peak is at 2101–2105 cm^{-1}, and the CD_2 ν_a peak is at 2195 cm^{-1}. The 100AzUDT spectrum intensity was reduced by half to fit within the absorbance window.

interface of SAMs and water; this must be measured by a subnanometer sensitive technique, such as NR.

Grazing Incidence Angle Reflection–Absorption Surface Fourier Transform Infrared Spectroscopy. GRAS–FTIR has been prominently used to evaluate SAM ordering, and it has implicitly become the consensus technique for concluding whether or not a SAM presents a close-packed structure. Using a p-polarized beam, FTIR absorption frequencies of SAM methylene stretches provide information on average chain ordering in a SAM structure.[1,12,18,55] In particular, the asymmetric methylene stretching frequency, ν_a, is correlated to the crystallinity of SAMs. Densely packed SAMs exhibit methylene asymmetric, ν_a, and symmetric, ν_s, modes similar to that of crystalline alkyl thiols (ν_a: 2918 cm^{-1}, ν_s: 2951 cm^{-1}) rather than bulk liquid (ν_a: 2924 cm^{-1}, ν_s: 2855 cm^{-1}).[8,18] Representative spectra for the prepared SAMs are shown in Figure 4, and all the frequencies recorded for each SAM are in Table S1.

The 100AzUDT spectrum (purple solid line, Figure 4A) exhibited an average ν_a at 2919.1 ± 1.3 cm^{-1} and ν_s at 2851 ± 3 cm^{-1}. These values are very similar to the modes found for crystallized alkyl thiols, implying well-formed SAMs with close-packed domains. In the case of 100DT (black solid line, Figure 4A), ν_a was located at 2919 ± 2 cm^{-1} and ν_s was located at 2848.0 ± 1.4 cm^{-1}, also indicating crystalline alkane thiols. GRAS–FTIR peak positions were directly dependent on the alkyl chain length; shorter chains exhibit higher methylene stretching frequencies, and the small shift observed (1 cm^{-1}) here was similar to those reported for fully assembled SAMs with 9–11 carbons.[8,18] The mixed 25AzUDT (blue solid line, Figure 4A) SAMs had methylene stretching frequencies centered at 2918.4 ± 1.5 cm^{-1} (ν_a) and 2849.2 ± 0.2 cm^{-1} (ν_s). Again, these results are characteristic of a close-packed structure, indicating that mixed SAMs formed crystalline-like domains and their formation was unaffected by the difference in their terminal groups. CH_2 stretching modes were also detected in the 100D21 spectrum (black dashed line, Figure 4A) associated with the H/D ratio of 0.05 calculated by mass spectrometry (data not shown) of the D21 thiol used to prepare SAMs.

Similar to its homologue, CD_2 stretching frequencies also indicate the degree of ordering in a SAM. In contrast to CH_2 modes, CD_2 modes are not as intense and occur at lower energies. Cabarcos et al. previously created a well-formed reference SAM with perdeuterated hexadecanethiol and reported the CD_2 ν_a and CD_2 ν_s modes to be 2194 and 2089 cm^{-1}, respectively.[56] Figure 4B displays the CD_2 and azide stretches measured for the SAMs. The ν_a mode of 100D21 was found at 2194.7 ± 0.4 cm^{-1}, just slightly blue-shifted on average from that of deuterated hexadecanethiol reported by Cabarcos et al., which can be attributed to the shorter carbon chain as discussed previously. A peak at 2089 cm^{-1} was not detected in any 100D21 spectra. However, this mode was less intense than the ν_a mode in the report by Cabarcos et al., and d_{21}-decanethiol has close to half the CD_2 groups of d_{34}-hexadecanethiol. Thus, all signal intensities were expected to be reduced compared to Cabarcos et al., which may be the cause of the undetectable CD_2 ν_s. In the same report, Cabarcos et al. also induced disorder in SAMs through the inclusion of ester groups, which resulted in an intensity reduction in the peak at 2089 cm^{-1}. It is possible that the missing ν_s peak in 100D21 could also indicate some degree of disorder, but it was also reported that a significant (+18 cm^{-1}) shift of ν_a occurred in disordered samples, which was not observed for 100D21. Because the 100D21 spectra do not have a significant ν_a shift, the absence of the ν_s peak in 100D21 was most likely due to the decrease in deuteration. From the FTIR data, primarily close-packed domains were present in the 100D21 sample.

GRAS–FTIR results indicated that the SAMs prepared for this study were comparable with many other reports of well-formed SAMs made in the same way. It is important to consider that GRAS–FTIR provides an averaged view of the surface area probed (micrometer scale to millimeter scale) and cannot infer fine differences in coverage, ordering, or defects. In fact, different lengths of SAMs with the same spectral peaks energies and widths have measurable differences in the number of defects when analyzed with chemical etching and STM methods.[15] This became more apparent with the samples characterized here once analyzed with NR, as discussed below.

Cathodic Stripping Voltammetry. It has been common to report quantitative SAM SC using cathodic stripping voltammetry because it was first published that alkyl thiols dissociate from Au surfaces in a one-electron process around −1.0 V (vs Ag/AgCl).[21,57] The exact peak potential varies with SAM length, pH of the electrolyte, Au crystal lattice structure, and SAM phase.[58–63] To quantify SC with cathodic stripping, cyclic voltammograms of all surfaces in this study were measured and representative voltammograms are given in the Supporting Information (Figure S1). Each voltammogram had one major peak potential at −1.05 V (versus Ag/AgCl) and one to two minor peaks between −1.10 and −1.32 V that are

DOI: 10.1021/acs.langmuir.9b00541
Langmuir XXXX, XXX, XXX–XXX

characteristic of SAMs of 10−20 carbons in length,[64] mixed SAMs,[59,61] and the presence of different Au facets on the surface.[65] The integrated charge under all peaks was used to determine the SCs and is reported in Table 1. Calculated SCs for every SAM composition were significantly less than the maximum packing density of a uniform close-packed SAM (4.5×10^{14} molecules cm^{-2}),[30] with the lowest value recorded for 100DT, which was calculated to be as little as 31 ± 7% of a fully packed monolayer. These values directly contradict the high SAM coverages indicated by FTIR and contact angle goniometry. XPS was used to confirm that the thiols were in fact predominantly chemisorbed to the surface (Figure S2) because reductive desorption would not have detected physisorbed thiols, whereas the other methods do not differentiate between the two states.

Table 1. Calculated Molecular SC of SAMs Varying in Different Compositions by Stripping at Potentials Greater Than −1.0 V (vs Ag/AgCl)[a]

SAM	molecules/cm^2 × 10^{14}	±	% theoretical
100D21	1.7	0.1	38%
100DT	1.4	0.3	31%
25BrUDT	2.2	0.1	49%
50BrUDT	2.3	0.1	52%
75BrUDT	2.2	0.1	48%
100AzUDT	2.5	0.2	57%
100BrUDT	2.6	0.4	57%
close-packed SAMs	4.5		100%

[a]Standard deviations are for at least three samples. Percent coverage is calculated as a fraction of a theoretical completely close-packed $(\sqrt{3} \times \sqrt{3})R30°$ structure reported for alkyl thiols on Au.

Excessively low calculated surface density has been described before using this method, specifically for SAMs that were fabricated on Au that was deposited on Si or glass.[21,52,66,67] However, the SAM literature is not consistent and others who have used cathodic stripping calculated greater than 100% coverage of SAMs prepared in a similar manner to these, attributing the extra charge to double-layer charging capacitance.[59,61,68] The disagreement in this field has not been thoroughly addressed, but it is possible that a simple one-electron reduction process described for SAMs on single-crystal Au(111) does not accurately describe the mechanism of the reduction of SAMs from Au deposited on Si. One can rationalize this by considering the complex nature of the reduction: not only do electrons flow to the sulfur atoms, the electrode surface, once completely covered with an insulating layer, requires charge to compensate the double-layer capacitance.[68,69] Thus, assuming a one-electron transfer in calculating the coverage based on the charge is an over-simplification, especially in the case of a complex, polycrystalline gold surface. In fact, n as a noninteger value may be most appropriate. It has been well documented that Au deposited on Si results in a polycrystalline surface with many grain boundaries[3] and microscopic roughness, both of which have been reported to increase SAM defects,[14,20] and it is possible that these surface features alter the mechanism of desorption, perhaps even pushing complete reduction outside of the available potential window. To further complicate these results, Pensa et al. reported significant differences in the mechanism of electrochemical desorption of thiols from Au as a function of chain length.[70] Thus, the results measured here may only be comparable to SAMs of similar alkyl chain length. NR also measured SAM surface densities, and the comparison between the NR and cathodic stripping results is discussed below in order to reconcile these results.

Electrochemical Measurements of Heterogeneous Electron Transfer. Microscopic SAM integrity can be evaluated by measuring electron transfer between a redox species in solution and the Au surface. A perfectly uniform SAM monolayer will block any charge transfer, and the resulting current will be strictly capacitive.[18] This blockage is due to a significant decrease in the rate of electron transfer from tunneling through the insulating layer, which decreases with increasing SAM chain length.[71] Experimentally, microscopic defects in a SAM, such as pinholes, grain boundaries, and disordered regions, perform like a sum of Au ultramicroelectrodes (UMEs). The overall shape of the voltammogram will look like that of a UME, presenting a greatly decreased current (compared to bare Au) with a sigmoidal shape because of radial diffusion as opposed to semi-infinite linear diffusion on macroelectrodes.[12] In contrast, significant defects in a poorly formed SAM, such as low SC, will result in a voltammogram shape similar to that of a macroelectrode.

For the CV measurements, the potential of a 1 mM $Fe(CN)_6^{3-}$ (in 1 M KCl) solution was cycled on bare Au and on the SAM between 0.5 and −0.2 V. Ferricyanide is reduced in a reversible, one-electron, outer-sphere redox reaction that is sensitive to the thickness of physical blocking layers on the electrode. Because of this, it has been used as an indicator of SAM SC.[13,17,18,59,72] Representative voltammograms for three

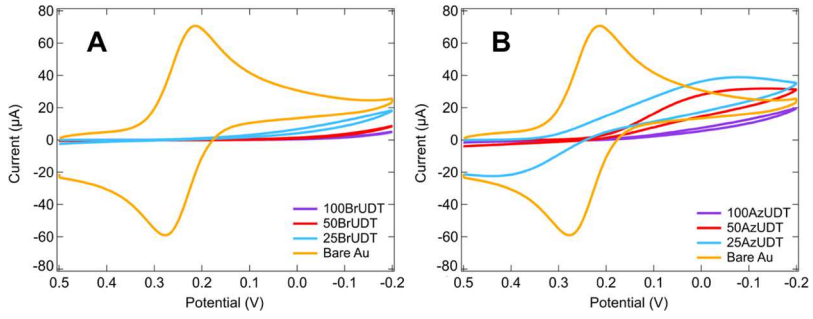

Figure 5. Representative CVs of 1 mM $Fe(CN)_6^{3-}$ in 1 M KCl on bare Au (orange), bromine-terminated SAMs, and post-azide reaction SAMs. (A) Mixed SAMs with Br-terminated alkyl thiols of 25% (blue) and 50% (red) Br-containing monolayers; the purple voltammogram represents a 100% Br-terminated SAM surface. (B) Representative CVs of $Fe(CN)_6^{3-}$ of 25AzUDT (blue), 50AzUDT (red), and 100AzUDT (purple) SAM surfaces.

DOI: 10.1021/acs.langmuir.9b00541
Langmuir XXXX, XXX, XXX−XXX

SAM compositions are shown in Figure 5. Voltammograms were collected from SAMs before and after exposure to NaN_3 (bromine- and azide-terminated, respectively). The Br-terminated SAMs (Figure 5A) blocked charge transfer from $Fe(CN)_6^{3-}$ efficiently, indicated by significant reduction in current from the SAM surface compared to the bare Au electrode and lack of peak potentials. The detected current is a combination of all possible electron tunneling pathways across the SAM.[14]

Representative CVs of $Fe(CN)_6^{3-}$ on azide-terminated SAMs are shown in Figure 5B; these CVs were both less reproducible and exhibited peak potentials in some samples. The azide-terminated SAMs blocked less charge than their brominated precursors. It was initially hypothesized that the azide reaction conditions destroyed the integrity of the SAM. However, FTIR analysis of SAMs before and after azide treatment show no changes in SAM structure and the contact angles of NaN_3-treated SAMs were reproducible (Figure 3). Significantly damaged SAM monolayers would not have reproducible contact angles, and their values would be much closer to that of bare Au. Furthermore, the charge measured from stripping 100BrUDT and 100AzUDT off of Au surfaces was not statistically different from one another (Table 1). Instead of destroying the SAM, it is more likely that the zwitterionic azide terminal groups and any unreacted azide salt remaining on the surface acted as an electron bridge between $Fe(CN)_6^{3-}$ and the Au surface. Enhanced electron transfer is known to occur in conjugated SAM systems,[73,74] and it is therefore plausible that the azide increased the rate of electron transfer across the SAMs. This mechanism would be augmented by any azide that was physisorbed to the Au surface at SAM defect sites.

To assess the extent of any NaN_3 that might be physisorbed to the surface, a cleaned and annealed bare Au surface was exposed to the same NaN_3 solution as a 100% Br-terminated SAM, 100BrUDT. After reaction, both the SAM and bare Au were rinsed vigorously in high-purity water and then DMF, which was repeated before the samples were finally rinsed in ethanol before drying under a stream of N_2(g). NaN_3 is highly soluble in water (65 g L^{-1} at 20 °C, Sigma-Aldrich Safety Data Sheet) and slightly soluble in DMF (7.3 g L^{-1} at 25 °C).[75] GRAS−FTIR of the bare Au surface after rinsing displayed a strong N_3 stretch at 2116 cm^{-1} (Figure 6), indicating the presence of NaN_3 on the bare Au surface. Additionally, the N_3 stretch for 100AzUDT at 2105 cm^{-1} has a clear shoulder at 2116 cm^{-1}, similar to the absorption energy of NaN_3 physisorbed on Au. These spectra revealed that unreacted NaN_3 was present on the bare Au surface and therefore likely on the 100AzUDT SAM surface as well. The detected NaN_3 on 100AzUDT reveals the ability of ions to penetrate the SAM, directly showing the presence of exposed Au from SAM defects. Our observation of adsorbed NaN_3 is in agreement with previous studies in which small ions passivate Au by traveling through SAMs of varying lengths.[12−15,17,20,76,77] Direct detection of remaining azide within the SAM supports our hypothesis that the decreased insulating character of the azide-reacted SAMs shown by CV is from azide-aided electron tunneling and not due to the loss of SAM structural integrity.

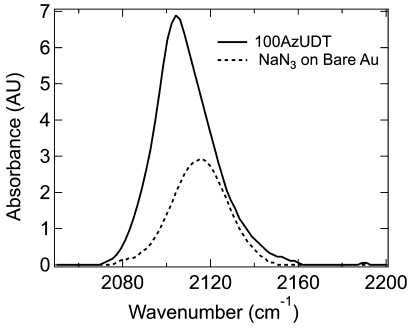

Figure 6. Ambient GRAS−FTIR spectra for 100AzUDT on Au (solid line) and bare Au exposed to the NaN_3 substitution reaction (dotted line). The N_3 stretch was located at 2104 and 2116 cm^{-1} for the SAM or NaN_3 physisorbed to Au, respectively.

Collectively, the FTIR, contact angle, and electrochemical results demonstrated well-formed monolayers representative of SAMs reported elsewhere. Although it is uncommon in the recent literature to recognize or discuss SAM defects and disorder, these molecular imperfections have been historically disclosed with many methods and are not unique to the SAMs studied here.[12−14,18,76−78] These experimental reports of SAM defects have relied on indirect methods to measure exposed Au surfaces and most have given no information on the penetration of solvent into these defects, which is an especially important property for SAMs meant to act as a physical barrier, for controlled electrochemistry, or for biological functionalization. It is necessary to quantify solvent intercalation in SAMs to generate a clearer picture of the molecular structure of the SAMs in a complex environment.

Neutron Reflectometry. NR measures the specular reflectivity of a multilaminar system, which is dependent on the thickness, interfacial roughness, and average chemical composition of each layer. In NR studies, the compositional density of each layer is expressed as the SLD (see eq 3), which is dependent on the coherent scattering length of each atom in the material as well as the molecular volume of each compound. SLDs of mixtures are a weighted average of SLDs of each compound in that layer. The isotopic sensitivity and subnanometer thickness resolutions of NR make it an ideal tool for directly measuring the interaction between SAMs and aqueous solvents. For the reflectivity studies, three different SAM compositions were analyzed: 25% 11-azido-1-undecanethiol, 75% d_{21}-decanethiol, 25AzUDT (D21); 50% 11-azido-1-undecanethiol, 50% d_{21}-decanethiol, 50AzUDT (D21); and 100% 11-azido-1-undecanethiol, 100AzUDT. An additional 100% 11-azido-1-undecanethiol SAM was analyzed, which was created with a presynthesized thiol (100AzUDT-p), in contrast to the other SAMs whose terminal azides were substituted post SAM formation on Au. Deuterated decanethiol was used because the SLD (5.99×10^{-6} $Å^{-2}$, liquid density) is significantly greater than hydrogenated decanethiol (-0.26×10^{-6} $Å^{-2}$, liquid density), creating a higher degree of contrast between the SAM and the layers surrounding it (Au and air/water). These SLD values were calculated using standard neutron scattering lengths and the manufacturer reported molar masses and densities (see eq 3).[49]

Raw reflectivity data as a function of Q for each SAM surface when dry and immersed in D_2O, H_2O, or 70/30 D_2O/H_2O (markers) along with Motofit fits (solid lines) are plotted in Figure 7A−D. The same data and the respective fits modeled with Webi are plotted in Figure S5. Reflectivity dropped after Q reached the critical edge of reflection on the silicon substrate and declined with increasing Q. The constructive and deconstructive interference between reflected neutrons traveling through the different layers above the silicon produced the

DOI: 10.1021/acs.langmuir.9b00541
Langmuir XXXX, XXX, XXX−XXX

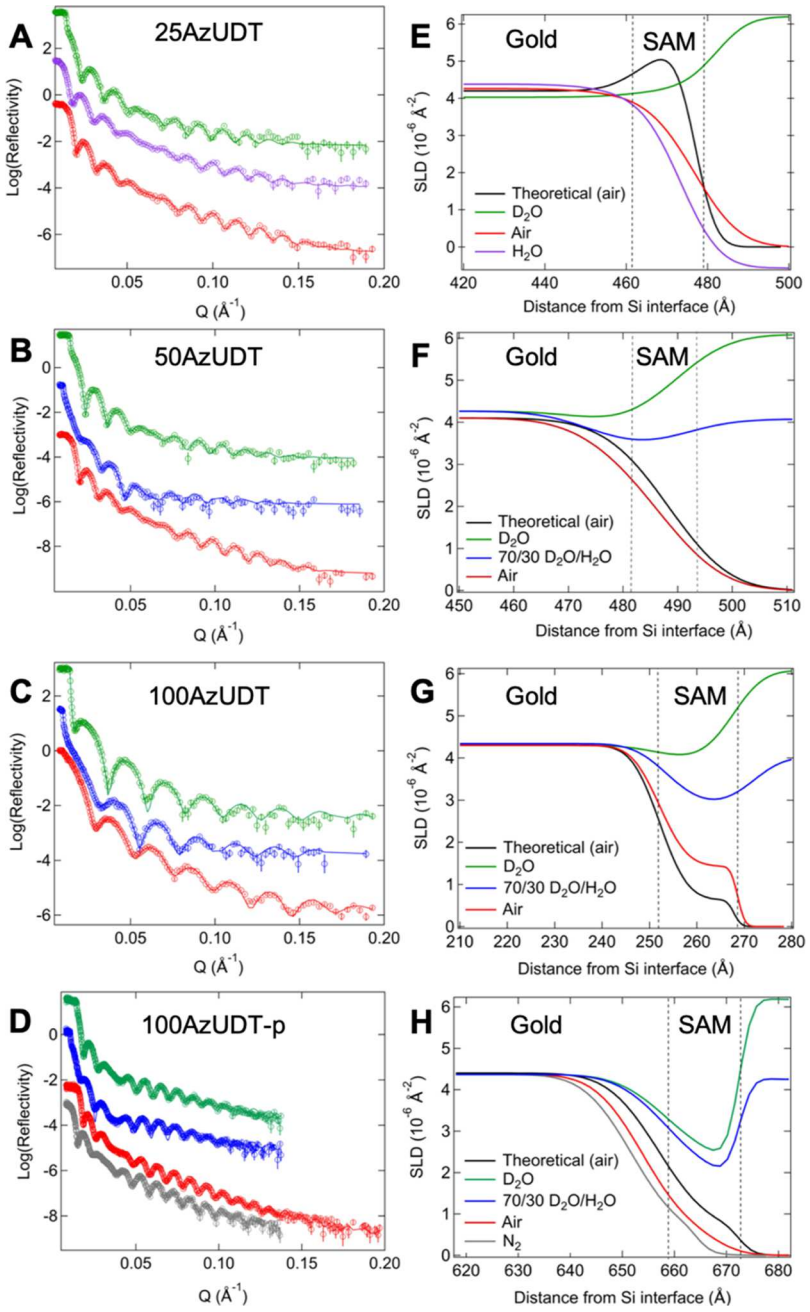

Figure 7. Reflectivity data (markers with associated error bars) and Motofit fits (solid lines) for (A) 25AzUDT in air (red, χ^2 = 1.9), H_2O (purple, χ^2 = 1.2), and D_2O (green, χ^2 = 4.0); (B) 50AzUDT mixed SAM in air (red, χ^2 = 2.3), 70/30 D_2O/H_2O (blue, χ^2 = 2.5), and D_2O (green, χ^2 = 2.1); (C) 100AzUDT in air (red, χ^2 = 2.9), 70/30 D_2O/H_2O (blue, χ^2 = 1.8), and D_2O (green, χ^2 = 1.8); (D) 100AzUDT-p in N_2 (gray, χ^2 = 1.8), in air (red, χ^2 = 2.3), 70/30 D_2O/H_2O (blue, χ^2 = 12.0), and D_2O (green, χ^2 = 2.9). Reflectivity profiles are vertically offset for visual clarity. SLD as a function of film depth is plotted for (E) 25AzUDT, (F) 50AzUDT, (G) 100AzUDT, and (H) 100AzUDT-p. Black lines in SLD plots were generated using the theoretical SLD value for a close-packed SAM of 100% coverage in air.

unique fringe patterns measured. For each sample, changes in the reflectivity profiles were discernable for each environment the sample was introduced to (blue, green, purple, gray, or red data in Figures 7A–D and S5). Best fit models were deduced for every data set using a single layer for the SAM. From these models, the SLD and thicknesses for each layer were extracted and graphed as a depth composition profile. Figure 7E–H are the SLD profiles from the Motofit models, scaled to highlight the SAM interface of interest.

The thickness, SLD, and roughness values for the inorganic layers obtained from NR models of each sample had to be in agreement across all environments. Refined models that fit all data sets for each sample produced the values listed in Table 2 (Motofit) and Table S3 (Webi) with the exception of the single-crystal Si substrate, in which the SLD was set to its documented value (2.07×10^{-6} Å^{-2}).[50] Because phase information is lost in neutron reflectivity experiments, it is possible that multiple models may be fit to the collected reflectivity profile. To ensure that the layered model generated to fit the reflectivity data was physically relevant, information about the samples collected using other analytical techniques was used to provide constraints during the modeling process.

DOI: 10.1021/acs.langmuir.9b00541
Langmuir XXXX, XXX, XXX−XXX

Table 2. Inorganic Layer Thicknesses (t), SLDs, and Roughness Values (r) Obtained from Motofit Models of NR Measurements[a]

parameter	25AzUDT (D21)	50AzUDT (D21)	100AzUDT	100AzUDT-p
SiO_x t (Å)	15.4 (0.6)	15.5 (0.8)	15.5 (0.4)	39.3 (1.1)
SiO_x SLD (10^{-6} Å^{-2})	2.72 (0.13)	2.46 (0.06)	3.95 (0.06)	2.96 (0.12)
SiO_x r (Å)	1.5 (0.2)	2.95 (0.05)	1.4 (0.2	1.85 (0.10)
Cr t (Å)	41 (3)	44.8 (1.6)	8.92 (0.15)	49 (2)
Cr SLD (10^{-6} Å^{-2})	3.02 (0.01)	3.00 (0.03)	2.99 (0.06)	2.91 (0.13)
Cr r (Å)	13.3 (0.4)	12.1 (1.4)	5.8 (0.1)	22.7 (0.8)
Au t (Å)	408 (2)	416 (2)	228 (1)	568 (7)
Au SLD (10^{-6} Å^{-2})	4.28 (0.18)	4.21 (0.09)	4.32 (0.02)	4.37 (0)
Au r (Å)	11.2 (0.6)	8.6 (0.2)	5.2 (0.5)	7.4 (0.2)

[a]Roughness is given as root-mean-square values. SiO_x thickness and SLD varied for each sample as a function of the wafer commercial source, likely due to the polishing methods used at different facilities. Values are averages between all models for each sample, and errors in parentheses are the respective standard deviations.

Additionally, each samples' reflectivity was measured in contrasting solvents (D_2O and H_2O/D_2O mixture or H_2O) to reduce ambiguity in the final wet models. Values for Au and Cr thicknesses determined from NR were consistent with those measured by QCM during the deposition process. The SLDs calculated for Cr were very close to the bulk value of 3.03×10^{-6} Å^{-2}, whereas the calculated SLDs of Au were slightly lower than its dense bulk value (4.5×10^{-6} Å^{-2}), which is consistent with what has been reported before.[29,43,79] A slightly reduced SLD for Au likely has two causes: (1) the deposition process results in polycrystalline Au with structural defects that reduce the Au density and (2) Cr is known to permeate Au in small amounts, which can reduce the average SLD.[14]

Thicknesses and SLD values obtained from best Motofit models for 25AzUDT, 50AzUDT, 100AzUDT, and 100AzUDT-p in all environments shown in Figure 7A–D are reported in Table 3. The error values in Table 3 represent the statistical uncertainty in each parameter obtained through Monte Carlo analysis rather than the physical error in the measurement. Theoretical SLDs were calculated using areal densities of close-packed, crystalline SAM domains and previously reported SAM heights.[30] Detailed calculations are available in the Supporting Information. The experimentally determined SLDs for native 25AzUDT and 50AzUDT SAMs in air (Tables 3 and S4) are lower than theoretical SLDs of 100% close-packed surfaces, indicating that the samples had a reduced level of surface density coverage. Thiol densities were calculated to be 68% for 25AzUDT and 73% for 50AzUDT by dividing the average between the experimental SLDs determined in Motofit and Webi with the theoretical, 100% close-packed coverage SLD. This ~30% deviation from the perfect uniform SAM coverage is the cumulative effect of defects inherent to SAMs, including Au step edges, SAM interdomain spacing, disordered or fluid SAM morphology, pinholes, or other defects. The 100AzUDT sample had an experimental SLD three times the expected value for 100% coverage. This deviation arises from the presence of residual NaN_3 physisorbed to the surface as a consequence of the SAM preparation process. NaN_3 has an SLD of 5.43×10^{-6} Å^{-2} (using bulk density), which raises the observed SLD of 100AzUDT proportionally by the amount of physisorbed azide salt. GRAS–FTIR showed that azide salt could strongly physisorb to bare Au surfaces as well as the 100AzUDT surface (Figure 6). We hypothesize that nanoscopic aggregates of NaN_3 accumulated in defects and perhaps to the surface of the SAM itself. This is supported by evidence that negatively charged halogens and cyanide adsorb strongly to Au surfaces,[12,20,80,81] and it is possible that the azide anion has a similar interaction with Au, making it more difficult to rinse away from buried SAM defects. Our observations of adsorbed NaN_3 are in agreement with previous studies in which small ions penetrate SAMs of varying lengths.[12–15,17,20,76,77] Finally, 100AzUDT-p was the equivalent SAM to 100AzUDT, but in this case, the azide terminus was synthesized on the thiol prior to SAM formation. This sample was never exposed to NaN_3 and therefore would not have any NaN_3 on the surface. Indeed, the SLD of 100AzUDT-p resulted in a calculated surface density of 76% compared to the theoretical value. This is similar to the surface densities of the other two SAM compositions and confirms the presence and effect of NaN_3 remaining on the 100AzUDT surface. If 100AzUDT had the same SAM surface density as 100AzUDT-p, the surface of 100AzUDT was 79% SAM and 21% NaN_3 by composition.

It is possible that 25AzUDT and 50AzUDT also had physisorbed NaN_3 on their surfaces. However, the amount of NaN_3 was found to be a function of the rinsing time and the percent azide termination of the SAM, with NaN_3 preferentially sticking to surfaces with higher AzUDT composition. This was discovered by measuring the area of the azide stretching peak at ~2104 cm^{-1} for 25AzUDT and 100AzUDT

Table 3. Thickness, t, and SLD Values Derived from Best Motofit Models for Different SAM Mixture Compositions and Theoretically Calculated Values[a]

SAM	theoretical SLD ($\times 10^{-6}$ Å^{-2})	dry SLD ($\times 10^{-6}$ Å^{-2})	D_2O SLD ($\times 10^{-6}$ Å^{-2})	contrast SLD ($\times 10^{-6}$ Å^{-2})	air t (Å)	D_2O t (Å)	contrast t (Å)
25AzUDT (D21)	5.46	3.75 (0.03)	4.49 (0.15)	3.69 (0.08) H_2O	14.4 (0.3)	11.9 (0.6)	11.9 (0.6) H_2O
50AzUDT (D21)	3.64	2.62 (0.09)	3.78 (0.04)	3.14 (0.05) 70/30	11.2 (0.2)	13.0 (0.2)	13.0 (0.1) 70/30
100AzUDT	0.63	1.45 (0.06)	3.98 (0.04)	2.91 (0.04) 70/30	16.5 (0.3)	16.5 (0.4)	18.3 (0.6) 70/30
100AzUDT-p	0.63	0.46 (0.06) air	2.25 (0.02)	1.84 (0.03) 70/30	15.2 (0.9) air	13.6 (0.1)	13.8 (0.2) 70/30
		0.50 (0.08) N_2			12.6 (0.5) N_2		

[a]Theoretical air SLDs represent a close-packed, 100% coverage SAM. All other SLD and thickness values were experimentally determined. Error values in parentheses are model confidences for the individual sample.

DOI: 10.1021/acs.langmuir.9b00541
Langmuir XXXX, XXX, XXX–XXX

exposed to standard rinsing and after rinsing time was increased by a factor of 8. Each spectrum was normalized to the CH_2 asymmetric stretch absorbance and the relative number of methylene groups for each SAM. When rinse times for SAMs were increased, the area of the azide peak decreased by 18% for 100AzUDT and 17% for 25AzUDT. Because the percent reduction is similar between both samples, the absolute amount of NaN_3 rinsed off of 25AzUDT can be approximated to one-fourth of the amount of NaN_3 that was rinsed off of 100AzUDT. AzUDT appears to favor the physisorption of NaN_3 on the SAM surfaces. The 25AzUDT and 50AzUDT surfaces measured by NR were prepared at a later time than 100AzUDT, and both the rinsing times and convection levels for these samples were significantly increased to remove excess NaN_3. Although the quantity of remaining NaN_3 bound to the 25AzUDT and 50AzUDT surfaces cannot be quantified, it was likely minimal in these two samples because they underwent a more rigorous wash and have lower azide termination.

One possibility for the observed low SAM surface density is that the measurements in air were affected by the presence of atmospheric humidity absorbing into the SAM. Water has an SLD of -0.56×10^{-6} Å^{-2} and hence absorbed water would lower the measured SAM SLD. To test this, 100AzUDT-p was measured under a constant flow of dry N_2(g) following its air measurement. The average SLD in N_2 between the Motofit model (Table 3) and Webi (Table S4) models was $0.49 \pm 0.09 \times 10^{-6}$ Å^{-2}, which is statistically the same as the SLD measured in air. This indicates that ambient levels of humidity or any other potential atmospheric contaminants did not affect the SAM SLD. The SAM density coverages calculated by NR are good estimates of the actual thiol coverage on the Au.

Because NR independently determined SAM SC, it is worth comparing these values to those determined by cathodic stripping voltammetry, which were discussed above. Unrealistically low coverages were calculated using cathodic stripping methods with the assumption that the thiol reduced in a one-electron process (see Table 1). Given this, we hypothesize that the desorption of thiols from polycrystalline gold is more complex than a one-electron reduction. Electrochemists prefer to describe complex chemisorption using "electrosorption valency", λ, instead of the number of electrons. λ is defined by eq 5

$$\lambda = \left(\frac{\partial q_m}{\partial \Gamma_s}\right)_E / F \tag{5}$$

where q_m is the thermodynamic charge density on the Au electrode, Γ_s is the quantity of thiol (adsorbate), E is the electrode potential, and F is Faraday's constant.[68] λ is useful because it can be used in place of the number of electrons, n, in the Nernst equation for an adsorbate system but does not have to be an integer number. More importantly, λ accounts for any partial charge transfers and double-layer capacitance in addition to Faradaic charge, making it superior for interpreting SAM desorption.[68] Considering the coverages determined by NR and the charges obtained with reductive desorption, λ was calculated to be 0.54 ± 0.06, 0.55 ± 0.06, and 0.55 ± 0.16 for 25AzUDT, 50AzUDT, and 100AzUDT, respectively. These values, like coverage, were lower than λ calculated by others for thiols on single-crystal metal substrates, but a more in-depth study to determine the individual contributing components of λ is required to draw any further conclusions.[68,69] It is important to emphasize, however, that SAM coverage on polycrystalline Au is not well resolved with cathodic stripping voltammetry. As stated previously, it is possible that the cathodic limit for complete desorption was not reached or was concealed by the hydrogen reduction current. This method's lack of accuracy is particularly noteworthy because the actual SAM coverage directly impacts the ability to interpret the interaction of solvent with the surface, the key question of this investigation.

Although there is literature evidence that small ions, often in aqueous solution, penetrate SAMs and adsorb to exposed Au, there are limited published experimental data confirming that water itself penetrates fully formed SAMs of alkyl thiols on gold. It is probable that if a small charged molecule can reach Au through SAM defects and pinholes, then water is likely to permeate SAMs of alkyl thiols on gold as well. To test this hypothesis directly with SAMs created by the most ubiquitous method and on the most commonly used substrate, NR was collected on SAMs immersed in D_2O and H_2O or 70/30 D_2O/H_2O solutions. Figure 7E–H highlights the Au/SAM/solvent interfaces of the SLD profiles that correspond to the respective reflectivity models. The SAM layer boundaries are indicated by vertical dashed lines for clarity. Interfacial roughness between Au/SAM and SAM/water (or air) results in the curvature of the lines seen between those layers, in which a completely smooth interface would manifest as a sharp 90° angle transition from one SLD value to the next. In these graphs, the SAM layer is best visualized by the samples immersed in 70/30 D_2O/H_2O (blue), which has roughly the same SLD value as Au.

A constant SLD value for each SAM regardless of environment would be expected for a system with uniform SAM coverage that acted as a perfect blocking layer between the Au surface and the air/aqueous environment. However, the SLD of the SAM varied depending on the environment it was exposed to, shown by the diverging SLDs at the Au/SAM interface in Figure 7E–H. Moreover, increases in the SLD of the SAM were correlated with increases in the SLD of the aqueous environment to which it was exposed. These changes in SLD values indicate that SAM composition was altered upon immersion in an aqueous environment, implying either intercalation of water molecules within the SAM network or water filling the void spaces of the exposed Au surface.

NR measured dramatic SLD changes that were environmentally dependent, directly indicating the presence of water in the SAM layer when immersed in solution. The SLDs, thicknesses, and model confidences in these values are listed in Table 3 for Motofit and Table S4 for Webi. To quantify the water associated with the SAM, the number of water molecules that scattered neutrons per thiol was calculated by eq 4 using the molecular volume of the SAM determined by the SLD in air. Molecular volume calculations are included in the Supporting Information. The number of water molecules per SAM is plotted in Figure 8 as a function of SAM composition. For each sample, the water/thiol ratio was calculated for each wet environment individually (Figure 8 blue, purple, and green bars) using the average SLD between Motofit and Webi for each environment. Water uptake calculated by NR was appreciable in each sample where the average numbers of water molecules were 1.6, 2.1, 5.7, and 4.6 per thiol of 25AzUDT, 50AzUDT, 100AzUDT, and 100AzUDT-p SAMs, respectively. This result was unsurprising given the coverage analysis of the SAMs measured in ambient air but is in stark

DOI: 10.1021/acs.langmuir.9b00541
Langmuir XXXX, XXX, XXX–XXX

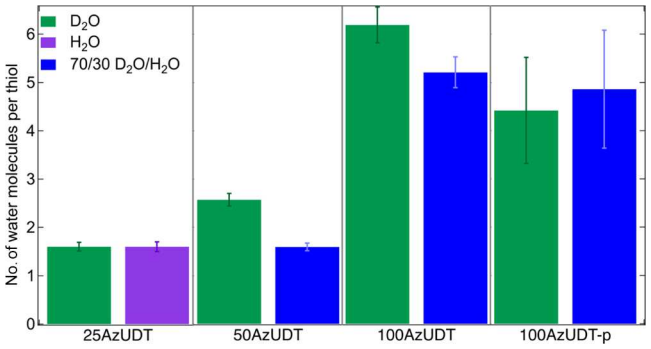

Figure 8. Number of water molecules per thiol calculated from the average between the Motofit and Webi wet model's SAM SLD value. Error bars represent propagated model confidences. Water quantity was determined using the SLD value of the SAM in D_2O (green), H_2O (purple), and 70/30 D_2O/H_2O (blue) compared to the experimental SAM SLD in air.

contrast to the typical assumption that SAMs are a uniform physical barrier between the underlying Au and solvent. This is especially true in the case of 25AzUDT, which was a distinctly hydrophobic surface according to contact angle measurements.

There are three possibilities for how this quantity of water would interact with SAMs: (1) water associates with the hydrophilic terminal azide groups; (2) water forms a nonbulk layer at the SAM/aqueous interface; or (3) water intercalates into defects and disordered regions of the SAM. Here, we evaluate these three possibilities in light of the accumulated evidence.

If association with terminal azide groups was the driving force for the presence of water, we would expect that the amount of water would increase with the AzUDT content of the SAM just as the contact angle measurements showed increases in overall hydrophilicity. However, the number of water molecules calculated per thiol is not physically consistent with the geometric constraints of the terminal group structure of the SAMs. In the most extreme case, 100AzUDT was calculated to have 5.7 waters per thiol chain, which, using bulk water density, correlates to a volume of 172 Å^3, 4.5 times larger than the azide terminus (38 Å^3). Additionally, in close-packed SAMs domains, neighboring azide termini can be as little as 5 Å from one another if they are aligned with the underlying sulfur atom. Steric hindrance would not allow such a large number of water molecules to orient around an individual azide group. While the average number of water molecules does increase with the azide content in the SAM, the trend does not linearly correlate with percent azide termination, implying that water molecule associated with terminal groups is not the dominant factor in driving water inclusion.

The second possibility, that a region of interfacial water that was chemically distinct from bulk water (and therefore had a different SLD than bulk water) because of disruptions in its hydrogen bonding network, was also explored. The thickness and density of a hypothesized density depletion layer in contact with hydrophobic surfaces have been measured and modeled multiple times but with inconsistent conclusions.[82,83] No models for any of the reflectivity data sets used to calculate water intercalation were able to fit to two layers, that is, one for a static SAM and one for a volume of nonbulk water (NBW). If there was an NBW layer above the SAM, the reflectivity would have captured it. However, if the NBW layer was thinner than the roughness values of the SAM or Au, then the SAM and NBW would not have been differentiable in our models. In this case, the SLD values for the SAM layer would have been a weighted average of the two compositions and the thickness of the whole layer would have included the SAM and NBW. Additionally, it would be expected that the SAM thicknesses would have been larger in the wet measurements than the dry measurements to accommodate the NBW layer. To determine if this is a reasonable explanation for the NR data, the expected thickness increase of the modeled SAM layer was calculated using bulk water density to be 33, 15, and 12% thicker for 100AzUDT, 50AzUDT, and 25AzUDT, respectively. However, a density depleted water layer would have a higher molecular volume, and therefore, the thickness increases would be larger than this. The NR reported thicknesses (Tables 3 and S4) do not fluctuate outside of the ∼10% systematic error expected for this method. Other NR measurements have resulted in similar layer thickness differences between separate measurements of the same sample.[84,85] The heights of the SAMs also do not consistently increase upon immersion into water. Taken together, the evidence does not support this possibility.

The third possibility considered water penetrating the SAM layer based on the molecular volume of water, as well as the affinity of water for Au in concert with the presence of defects gleaned from the ambient air NR, GRAS−FTIR, and heterogeneous electron-transfer measurements. The molecular volume of water (30 Å^3) is less than the molecular volumes of charged species that have been shown to penetrate SAMs, such as azide presented here (58 Å^3) and cyanide reported elsewhere (59 Å^3).[12] On the basis of size, it is not unreasonable to presume that water can also penetrate SAMs. Additionally, the underlying Au surface is inherently hydrophilic and completely wetted when introduced to a drop of water (advancing contact angle of 49.6 ± 1.5°), implying a thermodynamic advantage for water to be in contact with the Au surface, driving water to fill in gaps of the SAM. Because the thiol surface density was lower than an ideally close-packed SAM surface as a result of expected disorder and defects naturally occurring in alkyl thiols of this length formed on Au deposited on Si as demonstrated with heterogeneous electron transfer, we hypothesize that the water measured by NR was primarily located within the SAM at various sites including domain boundaries, pinholes, Au step edges, and disordered SAM domains.

The magnitude of water uptake by immersed SAMs was unexpected and enlightening. The data presented here provide a clear indication that SAMs are not a uniform, complete, physical barrier to the underlying Au but instead have inherent structural inhomogeneity after the self-assembly process. The quantity of water measured for the SAMs reported here is likely a combination of both water penetration at defect sites and some water association at the SAM/aqueous interface. To the best of our knowledge, this report is the first direct measurement of water absorbed into well-formed SAMs on Au. The possibility of water penetration in SAMs was first alluded to by Porter et al. as an explanation for the capacitance of alkyl thiols on Au to be slightly higher than on polyethylene because water uptake into the SAM layer would increase the dielectric of the material.[18] More recently, long-chain SAMs containing glycol groups, such as those used for protein antifouling surfaces, have been shown to absorb water into the hydrophilic, oxygen-containing regions of the SAM.[85−87] These results show that water molecules can penetrate past

DOI: 10.1021/acs.langmuir.9b00541
Langmuir XXXX, XXX, XXX−XXX

multiple levels of closely oriented methylene groups to hydrogen bond to ether oxygens, indicative of the flexibility of alkyl chains of SAMs. Additionally, the capability of water to imbed into the topmost methylene regions of alkyl SAMs has been supported by computational simulations.[38,88] These studies suggest that a small amount of water is able to move into the uppermost regions of SAMs, even in close-packed structures, because of the thermal movement of these methyl and methylene groups. This observation is likely a contributing factor to the quantity of water measured in this study.

In a comparable experiment to ours, vibrational sum frequency spectroscopy discovered that water was in direct contact with the fused silica substrate under intentionally disordered alkyl trichlorosilane monolayers.[89] Alkyl trichlorosilanes monolayers are similar to SAMs on gold in that they can also form ordered, standing-up domains, although with different organization, and are frequently used for similar purposes. These authors also found that advancing contact angles of water did not correlate to the presence or absence of water near the substrate, in agreement with the results of this study. Additionally, the methylene stretches of the highly ordered monolayers in those experiments were red-shifted when immersed in water, implying that water was at least in contact with the externally located methylene peaks because of the higher presence of gauche conformers in that area. These results endorse our hypothesis that water is primarily located in the disordered and defect areas of the submerged SAMs.

The water content of the SAMs calculated in this investigation implies a greater degree of defects than typically measured for SAMs using more indirect methods, including heterogeneous electron transfer and chemical etching. Using heterogeneous electron transfer, the fractional pinhole area in octadecanethiol monolayers on a polycrystalline Au (on Si) electrode was determined by Porter et al. to be $<6 \times 10^{-6}$ using $Fe(H_2O)_6^{3+}$ and $Fe(CN)_6^{3-}$ as the redox species.[18] That study also reported that decreasing the SAM chain length increased the amount of diffusion of the redox molecule through the SAM, implying an increased number of pinholes with the shorter alkyl chains. While pinhole coverage was not specifically calculated in this paper, it is expected that undecanethiol would have had a higher fraction of pinholes compared to octadecanethiol used in the Porter et al. study. It is worth considering that the redox species used by Porter et al. were significantly larger than individual water molecules; thus, it would be expected that the degree of water diffusion into the SAM would be greater than that of the redox species. Another method for measuring defects in SAMs is to chemically etch exposed Au until the underlying Si layer is exposed and then amplifying pinhole sizes by chemically etching Si before finally counting the number of amplified pinholes via STM imaging.[12,15,20] This technique has been used to quantify defect densities on the order of 5−120 etched pits per mm^2 depending on gold thickness, SAM preparation method, and chain length. Chemical etching provides a qualitative way to measure defect trends; however, the number of pinholes is likely underestimated because larger defects are favored by this process and STM suffers from the inability to capture the average structural condition of the entire sample unless a very large number of areas are probed.[20]

STM imaging has been the dominant tool for characterizing defects found in SAMs and is a direct method for doing so. STM images have been crucial to identifying the various types of defects, including interdomain boundaries, lying-down phases, amorphous regions of thiols, vacancy islands, pinholes, and missing rows.[90−94] It is within these well-characterized regions that we hypothesize water is infiltrating. Although STM has proved to be a powerful qualitative atomic-level characterization tool, it does not quantify the extent of defects on an entire surface, particularly one as large as that probed by NR (20 mm × 30 mm). Our results indicate that the defects within SAMs used in this study encompass ∼25% of the surface and, moreover, are penetrable to water in an aqueous environment.

NR is an appropriate tool for directly measuring water at SAM surfaces because of its unique isotopic sensitivity and subnanometer resolution of thicknesses of individual layers of the sample. The observation that water can be found within immersed SAMs in defect sites, disordered zones, and perhaps even in the more fluid terminal region is an important factor to be considered for the wide variety of SAM applications. As mentioned above, the SAM layer is rarely independently characterized and instead is assumed to be a uniform, completely covered monolayer of predominately ordered domains. The alkyl chain length, Au roughness, Au surface facets, SAM assembly time, and SAM assembly temperature all play a key role in SC and domain structure,[3,14] yet these features are frequently ignored when the focus of interest is post-SAM functionalization or chemistries.[42,95] Furthermore, the SAM is expected to act as a physical barrier between the underlying substrate and its exposed environment; however, structural defects can limit the functionality of SAM-based devices as they allow for a nontrivial amount of solvent diffusion to the Au surface. Steps to avoid SAM disorder, such as substrate choice, thiol length and terminal group selection, and solution purity are likely to minimize the permeability of a SAM to water; however, interdomain spaces, Au step edges, and pinholes have been detected in even the best SAM forming conditions and act as potential sites for solvent infiltration. The ubiquitous use of SAMs in a variety of research areas make these results notable and promote caution regarding their assumed uniformity, especially in techniques dependent on quantitative analysis such as their use as electrode surfaces for electrochemistry or as hydrophobic surfaces in density depletion layer investigations of water.

■ CONCLUSIONS

This study used NR to measure the water permeability of SAMs prepared using a common technique and supporting substrate. Results showed substantial water uptake into the SAM layer regardless of the hydrophobicity of the overall surface. The quality and properties of these SAMs were investigated by GRAS−FTIR, contact angle goniometry, cathodic stripping, and heterogeneous electron transfer and were found to be consistent with similarly prepared SAMs reported elsewhere. Water absorption in immersed SAMs conflicts with the frequently adopted notion that SAMs act as a physical barrier with a predominately hydrophobic, close-packed body. These findings suggest that the structure of commonly prepared SAMs represented by uniform, ordered domains cannot be automatically assumed and provide caution to researchers aiming to use SAMs as a homogeneous surface to quantitatively study adsorption or other surface interactions. Such discrepancies between the ideal and actual structures of SAMs could contribute to interpreting anomalous results concerning the coverage and structural stability of immobilized proteins on SAMs, why SAMs of this length scale are poor

DOI: 10.1021/acs.langmuir.9b00541
Langmuir XXXX, XXX, XXX−XXX

redox molecule blockers, why there are conflicting observations for water density depletion layers above hydrophobic SAMs, and other unexplained nanoscale observations in SAM-based aqueous systems.

■ ASSOCIATED CONTENT

Supporting Information

The Supporting Information is available free of charge on the ACS Publications website at DOI: 10.1021/acs.langmuir.9b00541.

Representative voltammograms of cathodic stripping of SAMs; values of all FTIR shifts in every SAM spectrum; XPS analysis of Au−thiolate bond; electrochemical determination of the Au surface area; atomic force microscopy images of Au substrates; calculations for theoretical SLDs and experimental molecular volumes of SAMs; Webi fits and tabulated parameter values; and NR analysis of 25AzUDT in 70/30 D_2O/H_2O (PDF)

■ AUTHOR INFORMATION

Corresponding Author

*E-mail: lwebb@cm.utexas.edu.

ORCID

Jason W. Dugger: 0000-0002-1196-0205
Jeffrey E. Dick: 0000-0002-4538-9705
Mathieu Doucet: 0000-0002-5560-6478
Lauren J. Webb: 0000-0001-9999-5500

Notes

The authors declare no competing financial interest.

■ ACKNOWLEDGMENTS

This research was supported through grants awarded by the National Science Foundation (CHE-1361252 and CHE-1807215 to L.J.W. and DGE-1110007 to J.E.D.) and Army Research Office (W911NF-17-1-0089 to L.J.W.). The research at Oak Ridge National Laboratory's Spallation Neutron Source was sponsored by the Scientific User Facilities Division, Office of Basic Energy Sciences, U.S. Department of Energy. The authors acknowledge the NIST/CNST NanoFab facility for providing Si wafers coated with smooth Au. The authors are also grateful for the instrumental resources provided by the Texas Materials Institute at the University of Texas at Austin in addition to the electrochemical setup loaned by the University of Texas at Austin's teaching laboratory stockroom.

■ REFERENCES

(1) Nuzzo, R. G.; Allara, D. L. Adsorption of Bifunctional Organic Disulfides on Gold Surfaces. *J. Am. Chem. Soc.* **1983**, *105*, 4481−4483.

(2) Bain, C. D.; Troughton, E. B.; Tao, Y. T.; Evall, J.; Whitesides, G. M.; Nuzzo, R. G. Formation of Monolayer Films by the Spontaneous Assembly of Organic Thiols from Solution onto Gold. *J. Am. Chem. Soc.* **1989**, *111*, 321−335.

(3) Love, J. C.; Estroff, L. A.; Kriebel, J. K.; Nuzzo, R. G.; Whitesides, G. M. Self-Assembled Monolayers of Thiolates on Metals as a Form of Nanotechnology. *Chem. Rev.* **2005**, *105*, 1103−1170.

(4) Vericat, C.; Vela, M. E.; Benitez, G.; Carro, P.; Salvarezza, R. C. Self-Assembled Monolayers of Thiols and Dithiols on Gold: New Challenges for a Well-Known System. *Chem. Soc. Rev.* **2010**, *39*, 1805−1834.

(5) Smalley, J. F.; Sachs, S. B.; Chidsey, C. E. D.; Dudek, S. P.; Sikes, H. D.; Creager, S. E.; Yu, C. J.; Feldberg, S. W.; Newton, M. D. Interfacial Electron-Transfer Kinetics of Ferrocene through Oligophenyleneethynylene Bridges Attached to Gold Electrodes as Constituents of Self-Assembled Monolayers: Observation of a Nonmonotonic Distance Dependence. *J. Am. Chem. Soc.* **2004**, *126*, 14620−14630.

(6) Harder, P.; Grunze, M.; Dahint, R.; Whitesides, G. M.; Laibinis, P. E. Molecular Conformation in Oligo(Ethylene Glycol)-Terminated Self-Assembled Monolayers on Gold and Silver Surfaces Determines Their Ability To Resist Protein Adsorption. *J. Phys. Chem. B* **1998**, *102*, 426−436.

(7) Dubois, L.; Nuzzo, R. G. Synthesis, Structure, and Properties of Model Oraganic Surfaces. *Annu. Rev. Phys. Chem.* **1992**, *43*, 437−463.

(8) Dubois, L. H.; Zegarski, B. R.; Nuzzo, R. G. Molecular Ordering of Organosulfur Compounds on Au(111) and Au(100): Adsorption from Solution and in Ultrahigh Vacuum. *J. Chem. Phys.* **1993**, *98*, 678−688.

(9) Raigoza, A. F.; Fies, W.; Lim, A.; Onyirioha, K.; Webb, L. J. One-Pot Reaction for the Preparation of Biofunctionalized Self-Assembled Monolayers on Gold Surfaces. *Appl. Surf. Sci.* **2017**, *394*, 288−296.

(10) Zhang, S.; Maidenberg, Y.; Luo, K.; Koberstein, J. T. Adjusting the Surface Areal Density of Click-Reactive Azide Groups by Kinetic Control of the Azide Substitution Reaction on Bromine-Functional SAMs. *Langmuir* **2014**, *30*, 6071−6078.

(11) Badia, A.; Lennox, R. B.; Reven, L. A Dynamic View of Self-Assembled Monolayers. *Acc. Chem. Res.* **2000**, *33*, 475−481.

(12) Chailapakul, O.; Sun, L.; Xu, C.; Crooks, R. M. Interactions between Organized, Surface-Confined Monolayers and Vapor-Phase Probe Molecules. 7. Comparison of Self-Assembling n-Alkanethiol Monolayers Deposited on Gold from Liquid and Vapor Phases. *J. Am. Chem. Soc.* **1993**, *115*, 12459−12467.

(13) Chailapakul, O.; Crooks, R. M. Synthesis and characterization of simple self-assembling, nanoporous monolayer assemblies: a new strategy for molecular recognition. *Langmuir* **1993**, *9*, 884−888.

(14) Creager, S. E.; Hockett, L. A.; Rowe, G. K. Consequences of microscopic surface roughness for molecular self-assembly. *Langmuir* **1992**, *8*, 854−861.

(15) Zamborini, F. P.; Crooks, R. M. Corrosion Passivation of Gold byn-Alkanethiol Self-Assembled Monolayers: Effect of Chain Length and End Group. *Langmuir* **1998**, *14*, 3279−3286.

(16) Finklea, H. O.; Hanshew, D. D. Electron-Transfer Kinetics in Organized Thiol Monolayers with Attached Pentaammine(Pyridine) Ruthenium Redox Centers. *J. Am. Chem. Soc.* **1992**, *114*, 3173−3181.

(17) Chidsey, C. E. D.; Loiacono, D. N. Chemical Functionality in Self-Assembled Monolayers: Structural and Electrochemical Properties. *Langmuir* **1990**, *6*, 682−691.

(18) Porter, M. D.; Bright, T. B.; Allara, D. L.; Chidsey, C. E. D. Spontaneously organized molecular assemblies. 4. Structural characterization of n-alkyl thiol monolayers on gold by optical ellipsometry, infrared spectroscopy, and electrochemistry. *J. Am. Chem. Soc.* **1987**, *109*, 3559−3568.

(19) Chidsey, C. E. D. Free Energy and Temperature Dependence of Electron Transfer at the Metal-Electrolyte Interface. *Science* **1991**, *251*, 919−922.

(20) Zhao, X.-M.; Wilbur, J. L.; Whitesides, G. M. Using Two-Stage Chemical Amplification To Determine the Density of Defects in Self-Assembled Monolayers of Alkanethiolates on Gold. *Langmuir* **1996**, *12*, 3257−3264.

(21) Widrig, C. A.; Chung, C.; Porter, M. D. The Electrochemical Desorption of N-Alkanethiol Monolayers from Polycrystalline Au and Ag Electrodes. *J. Electroanal. Chem.* **1991**, *310*, 335−359.

(22) Schönenberger, C.; Sondag-Huethorst, J. A. M.; Jorritsma, J.; Fokkink, L. G. J. What Are the "Holes" in Self-Assembled Monolayers of Alkanethiols on Gold? *Langmuir* **1994**, *10*, 611−614.

(23) Lu, X.; Lv, B.; Xue, Z.; Li, M.; Zhang, L.; Kang, J. Self-Assembled Monolayers of a Thiol-Derivatized Porphyrin on Gold Electrode: Film Formation and Electrocatalytic Dioxygen Reaction. *Thin Solid Films* **2005**, *488*, 230−235.

(24) Park, W.; Hong, H. G. Determination of Reorganization Energy from the Temperature Dependence of Electron Transfer Rate Constant for Hydroquinone-Tethered Self-Assembled Monolayers (SAMs). *Bull. Korean Chem. Soc.* **2006**, *27*, 381−385.

DOI: 10.1021/acs.langmuir.9b00541
Langmuir XXXX, XXX, XXX−XXX

(25) Mie, Y.; Tateyama, E.; Komatsu, Y. P-Aminothiophenol Modification on Gold Surface Improves Stability for Electrochemically Driven Cytochrome P450 Microsome Activity. *Electrochim. Acta* **2014**, *115*, 364−369.
(26) Sosna, M.; Fapyane, D.; Ferapontova, E. E. Reconstitution of Peroxidase onto Hemin-Terminated Alkanethiol Self-Assembled Monolayers on Gold. *J. Electroanal. Chem.* **2014**, *728*, 18−25.
(27) Gutierrez-Sanchez, C.; Ciaccafava, A.; Blanchard, P. Y.; Monsalve, K.; Giudici-Orticoni, M. T.; Lecomte, S.; Lojou, E. Efficiency of Enzymatic O2 Reduction by Myrothecium verrucaria Bilirubin Oxidase Probed by Surface Plasmon Resonance, PMIRRAS, and Electrochemistry. *ACS Catal.* **2016**, *6*, 5482−5492.
(28) Krassen, H.; Stripp, S.; von Abendroth, G.; Ataka, K.; Happe, T.; Heberle, J. Immobilization of the [FeFe]-Hydrogenase CrHydA1 on a Gold Electrode: Design of a Catalytic Surface for the Production of Molecular Hydrogen. *J. Biotechnol.* **2009**, *142*, 3−9.
(29) Smith, M. B.; McGillivray, D. J.; Genzer, J.; Lösche, M.; Kilpatrick, P. K. Neutron Reflectometry of Supported Hybrid Bilayers with Inserted Peptide. *Soft Matter* **2010**, *6*, 862−865.
(30) Widrig, C. A.; Alves, C. A.; Porter, M. D. Scanning Tunneling Microscopy of Ethanethiolate and N-Octadecanethiolate Monolayers Spontaneously Adsorbed at Gold Surfaces. *J. Am. Chem. Soc.* **1991**, *113*, 2805−2810.
(31) Ulman, A.; Eilers, J. E.; Tillman, N. Packing and Molecular Orientation of Alkanethiol Monolayers on Gold Surfaces. *Langmuir* **1989**, *5*, 1147−1152.
(32) Allara, D. L.; Nuzzo, R. G. Spontaneously organized molecular assemblies. 2. Quantitative infrared spectroscopic determination of equilibrium structures of solution-adsorbed n-alkanoic acids on an oxidized aluminum surface. *Langmuir* **1985**, *1*, 52−66.
(33) Offord, D. A.; John, C. M.; Griffin, J. H. Contact Angle Goniometry, Ellipsometry, XPS, and TOF-SIMS Analysis of Gold-Supported, Mixed Self-Assembled Monolayers Formed from Mixed Dialkyl Disulfides. *Langmuir* **1994**, *10*, 761−766.
(34) Bain, C. D.; Biebuyck, H. A.; Whitesides, G. M. Comparison of Self-Assembled Monolayers on Gold: Coadsorption of Thiols and Disulfides. *Langmuir* **1989**, *5*, 723−727.
(35) Jia, J.; Mukherjee, S.; Hamoudi, H.; Nannarone, S.; Pasquali, L.; Esaulov, V. A. Lying-Down to Standing-Up Transitions in Self Assembly of Butanedithiol Monolayers on Gold and Substitutional Assembly by Octanethiols. *J. Phys. Chem. C* **2013**, *117*, 4625−4631.
(36) Millone, M. A. D.; Hamoudi, H.; Rodríguez, L.; Rubert, A.; Benítez, G. A.; Vela, M. E.; Salvarezza, R. C.; Gayone, J. E.; Sánchez, E. A.; Grizzi, O.; et al. Self-Assembly of Alkanedithiols on Au(111) from Solution: Effect of Chain Length and Self-Assembly Conditions. *Langmuir* **2009**, *25*, 12945−12953.
(37) Löfgren, J.; Grönbeck, H.; Moth-Poulsen, K.; Erhart, P. Understanding the Phase Diagram of Self-Assembled Monolayers of Alkanethiolates on Gold. *J. Phys. Chem. C* **2016**, *120*, 12059−12067.
(38) Kanduč, M.; Schlaich, A.; Schneck, E.; Netz, R. R. Water-Mediated Interactions between Hydrophilic and Hydrophobic Surfaces. *Langmuir* **2016**, *32*, 8767−8782.
(39) Whitesides, G. M.; Laibinis, P. E. Wet Chemical Approaches to the Characterization of Organic Surfaces: Self-Assembled Monolayers, Wetting, and the Physical-Organic Chemistry of the Solid-Liquid Interface. *Langmuir* **1990**, *6*, 87−96.
(40) Lee, T. R.; Carey, R. I.; Biebuyck, H. A.; Whitesides, G. M. The Wetting of Monolayer Films Exposing Ionizable Acids and Bases. *Langmuir* **1994**, *10*, 741−749.
(41) Yim, H.; Kent, M. S.; Huber, D. L.; Satija, S.; Majewski, J.; Smith, G. S. Conformation of End-Tethered PNIPAM Chains in Water and in Acetone by Neutron Reflectivity. *Macromolecules* **2003**, *36*, 5244−5251.
(42) Tarasevich, B. J.; Perez-Salas, U.; Masica, D. L.; Philo, J.; Kienzle, P.; Krueger, S.; Majkrzak, C. F.; Gray, J. L.; Shaw, W. J. Neutron Reflectometry Studies of the Adsorbed Structure of the Amelogenin, LRAP. *J. Phys. Chem. B* **2013**, *117*, 3098−3109.
(43) Perez-Salas, U. A.; Faucher, K. M.; Majkrzak, C. F.; Berk, N. F.; Krueger, S.; Chaikof, E. L. Characterization of a Biomimetic Polymeric Lipid Bilayer by Phase Sensitive Neutron Reflectometry†. *Langmuir* **2003**, *19*, 7688−7694.
(44) Yang, H.; Kwon, Y.; Kwon, T.; Lee, H.; Kim, B. J. "Click" Preparation of CuPt Nanorod-Anchored Graphene Oxide as a Catalyst in Water. *Small* **2012**, *8*, 3161−3168.
(45) Parratt, L. G. Surface Studies of Solids by Total Reflection of X-Rays. *Phys. Rev.* **1954**, *95*, 359−369.
(46) Nelson, A. Motofit- integrating neutron reflectometry acquisition, reduction and analysis into one, easy to use, package. *J. Phys.: Conf. Ser.* **2010**, *251*, 012094.
(47) Doucet, M.; Ferraz Leal, R. M.; Hobson, T. C. Web Interface for Reflectivity Fitting. *SoftwareX* **2018**, *7*, 287−293.
(48) Kienzle, P. A.; O'Donovan, K. V.; Ankner, J. F.; Berk, N. F.; Majkrzak, C. F. *REFL1D*, https://github.com/reflectometry/refl1d, 2018.
(49) Nelson, A. Co-refinement of multiple-contrast neutron/X-ray reflectivity data usingMOTOFIT. *J. Appl. Crystallogr.* **2006**, *39*, 273−276.
(50) Sears, V. F. Neutron Scattering Lengths and Cross Sections. *Neutron News* **1992**, *3*, 26−37.
(51) Gallardo, I. F.; Webb, L. J. Tethering Hydrophobic Peptides to Functionalized Self-Assembled Monolayers on Gold through Two Chemical Linkers Using the Huisgen Cycloaddition. *Langmuir* **2010**, *26*, 18959−18966.
(52) Sondag-Huethorst, J. A. M.; Fokkink, L. G. J. Potential-Dependent Wetting of Octadecanethiol-Modified Polycrystalline Gold Electrodes. *Langmuir* **1992**, *8*, 2560−2566.
(53) Ge, Z.; Cahill, D. G.; Braun, P. V. Thermal Conductance of Hydrophilic and Hydrophobic Interfaces. *Phys. Rev. Lett.* **2006**, *96*, 186101.
(54) Wang, H.; Chen, S.; Li, L.; Jiang, S. Improved Method for the Preparation of Carboxylic Acid and Amine Terminated Self-Assembled Monolayers of Alkanethiolates. *Langmuir* **2005**, *21*, 2633−2636.
(55) Nuzzo, R. G.; Dubois, L. H.; Allara, D. L. Fundamental Studies of Microscopic Wetting on Organic Surfaces. 1. Formation and Structural Characterization of a Self-Consistent Series of Polyfunctional Organic Monolayers. *J. Am. Chem. Soc.* **1990**, *112*, 558−569.
(56) Cabarcos, O. M.; Shaporenko, A.; Weidner, T.; Uppili, S.; Dake, L. S.; Zharnikov, M.; Allara, D. L. Physical and Electronic Structure Effects of Embedded Dipoles in Self-Assembled Monolayers: Characterization of Mid-Chain Ester Functionalized Alkanethiols on Au{111}. *J. Phys. Chem. C* **2008**, *112*, 10842−10854.
(57) Sumi, T.; Wano, H.; Uosaki, K. Electrochemical Oxidative Adsorption and Reductive Desorption of a Self-Assembled Monolayer of Decanethiol on the Au(111) Surface in KOH+ethanol Solution. *J. Electroanal. Chem.* **2003**, *550*−*551*, 321−325.
(58) Chaudhari, V.; Kotresh, H. M. N.; Srinivasan, S.; Esaulov, V. A.; Esaulov, V. A. Substitutional Self-Assembly of Alkanethiol and Selenol SAMs from a Lying-Down Doubly Tethered Butanedithiol SAM on Gold. *J. Phys. Chem. C* **2011**, *115*, 16518−16523.
(59) Meunier-prest, R.; Legay, G.; Raveau, S.; Chiffot, N.; Finot, E. Potential-Assisted Deposition of Mixed Alkanethiol Self-Assembled Monolayers. *Electrochim. Acta* **2010**, *55*, 2712−2720.
(60) Azzaroni, O.; Vela, M. E.; Andreasen, G.; Carro, P.; Salvarezza, R. C. Electrodesorption Potentials of Self-Assembled Alkanethiolate Monolayers on Ag(111) and Au(111). An Electrochemical, Scanning Tunneling Microscopy and Density Functional Theory Study. *J. Phys. Chem. B* **2002**, *106*, 12267−12273.
(61) Sawaguchi, T.; Sato, Y.; Mizutani, F. In Situ STM Imaging of Individual Molecules in Two-Component Self-Assembled Monolayers of 3-Mercaptopropionic Acid and 1-Decanethiol on Au(111). *J. Electroanal. Chem.* **2001**, *496*, 50−60.
(62) Hobara, D.; Ota, M.; Imabayashi, S.-i.; Niki, K.; Kakiuchi, T. Phase Separation of Binary Self-Assembled Thiol Monolayers Composed of 1-Hexadecanethiol and 3-Mercaptopropionic Acid on Au(111) Studied by Scanning Tunneling Microscopy and Cyclic Voltammetry. *J. Electroanal. Chem.* **1998**, *444*, 113−119.

DOI: 10.1021/acs.langmuir.9b00541
Langmuir XXXX, XXX, XXX−XXX

(63) Yang, D.-F.; Wilde, C. P.; Morin, M. Electrochemical Desorption and Adsorption of Nonyl Mercaptan at Gold Single Crystal Electrode Surfaces. *Langmuir* **1996**, *12*, 6570−6577.
(64) Thom, I.; Buck, M. On the Interpretation of Multiple Waves in Cyclic Voltammograms of Self-Assembled Monolayers of n-Alkane Thiols on Gold. *Z. Phys. Chem.* **2008**, *222*, 739−754.
(65) Xiao, X.; Li, H.; Wang, M.; Zhang, K.; Si, P. Examining the Effects of Self-Assembled Monolayers on Nanoporous Gold Based Amperometric Glucose Biosensors. *Analyst* **2014**, *139*, 488−494.
(66) Calvente, J. J.; Kováčová, Z.; Sanchez, M. D.; Andreu, R.; Fawcett, W. R. Desorption of Spontaneously Adsorbed and Electrochemically Readsorbed 2-Mercaptoethanesulfonate on Au(111). *Langmuir* **1996**, *12*, 5696−5703.
(67) Kondo, T.; Sumi, T.; Uosaki, K. A Rotating Gold Ring-Gold Disk Electrode Study on Electrochemical Reductive Desorption and Oxidative Readsorption of a Self-Assembled Monolayer of Dodecanethiol. *J. Electroanal. Chem.* **2002**, *538*−*539*, 59−63.
(68) Schneider, T. W.; Buttry, D. A. Electrochemical Quartz Crystal Microbalance Studies of Adsorption and Desorption of Self-Assembled Monolayers of Alkyl Thiols on Gold. *J. Am. Chem. Soc.* **1993**, *115*, 12391−12397.
(69) Guidelli, R.; Schmickler, W. Electrosorption Valency and Partial Charge Transfer. *Modern Aspects of Electrochemistry*; Springer, 2006; pp 303−371.
(70) Pensa, E.; Vericat, C.; Grumelli, D.; Salvarezza, R. C.; Park, S. H.; Longo, G. S.; Szleifer, I.; Méndez De Leo, L. P. New Insight into the Electrochemical Desorption of Alkanethiol SAMs on Gold. *Phys. Chem. Chem. Phys.* **2012**, *14*, 12355−12367.
(71) Adams, D. M.; Brus, L.; Chidsey, C. E. D.; Creager, S.; Creutz, C.; Kagan, C. R.; Kamat, P. V.; Lieberman, M.; Lindsay, S.; Marcus, R. A.; et al. Charge Transfer on the Nanoscale: Current Status. *J. Phys. Chem. B* **2003**, *107*, 6668−6697.
(72) Cannes, C.; Kanoufi, F.; Bard, A. J. Cyclic Voltammetric and Scanning Electrochemical Microscopic Study of Menadione Permeability through a Self-Assembled Monolayer on a Gold Electrode. *Langmuir* **2002**, *18*, 8134−8141.
(73) Tour, J. M.; Jones, L.; Pearson, D. L.; Lamba, J. J. S.; Burgin, T. P.; Whitesides, G. M.; Allara, D. L.; Parikh, A. N.; Atre, S. Self-Assembled Monolayers and Multilayers of Conjugated Thiols, .alpha.,.omega.-Dithiols, and Thioacetyl-Containing Adsorbates. Understanding Attachments between Potential Molecular Wires and Gold Surfaces. *J. Am. Chem. Soc.* **1995**, *117*, 9529−9534.
(74) Tivanski, A. V.; He, Y.; Borguet, E.; Liu, H.; Walker, G. C.; Waldeck, D. H. Conjugated Thiol Linker for Enhanced Electrical Conduction of Gold−Molecule Contacts. *J. Phys. Chem. B* **2005**, *109*, 5398−5402.
(75) Alexander, R.; Ko, E. C. F.; Mac, Y. C.; Parker, A. J. Solvation of Ions. XI. Solubility Products and Instability Constants in Water Methanol, Formamide, Dimethylformamide, Dimethylacetamide, Dimethyl Sulfoxide, Acetonitrile, and Hexamethylphosphorotriamide. *J. Am. Chem. Soc.* **1967**, *89*, 3703−3712.
(76) Finklea, H. O.; Snider, D. A.; Fedyk, J. Passivation of pinholes in octadecanethiol monolayers on gold electrodes by electrochemical polymerization of phenol. *Langmuir* **1990**, *6*, 371−376.
(77) Finklea, H. O.; Avery, S.; Lynch, M.; Furtsch, T. Blocking Oriented Monolayers of Alkyl Mercaptans on Gold Electrodes. *Langmuir* **1987**, *3*, 409−413.
(78) Meuse, C. W.; Niaura, G.; Lewis, M. L.; Plant, A. L. Assessing the Molecular Structure of Alkanethiol Monolayers in Hybrid Bilayer Membranes with Vibrational Spectroscopies. *Langmuir* **1998**, *14*, 1604−1611.
(79) Steichen, M.; Brouette, N.; Buess-Herman, C.; Fragneto, G.; Sferrazza, M. Interfacial Behavior of a Hairpin DNA Probe Immobilized on Gold Surfaces. *Langmuir* **2009**, *25*, 4162−4167.
(80) Gao, P.; Patterson, M. L.; Tadayyoni, M. A.; Weaver, M. J. Gold as a Ubiquitous Substrate for Intense Surface-Enhanced Raman Scattering. *Langmuir* **1985**, *1*, 173−176.
(81) Gao, P.; Weaver, M. J. Metal-Adsorbate Vibrational Frequencies as a Probe of Surface Bonding: Halides and Pseudohalides at Gold Electrodes. *J. Phys. Chem.* **1986**, *90*, 4057−4063.
(82) Maccarini, M.; Steitz, R.; Himmelhaus, M.; Fick, J.; Tatur, S.; Wolff, M.; Grunze, M.; Janeček, J.; Netz, R. R. Density Depletion at Solid−Liquid Interfaces: a Neutron Reflectivity Study. *Langmuir* **2007**, *23*, 598−608.
(83) Skoda, M. W. A.; Schreiber, F.; Jacobs, R. M. J.; Webster, J. R. P.; Wolff, M.; Dahint, R.; Schwendel, D.; Grunze, M. Protein Density Profile at the Interface of Water with Oligo(ethylene glycol) Self-Assembled Monolayers. *Langmuir* **2009**, *25*, 4056−4064.
(84) Akers, P. W.; Dingley, A. J.; Swift, S.; Nelson, A. R. J.; Martin, J.; Mcgillivray, D. J. Using Neutron Reflectometry to Characterize Antimicrobial Protein Surface Coatings. *J. Phys. Chem. B* **2017**, *121*, 5908−5916.
(85) Schwendel, D.; Hayashi, T.; Dahint, R.; Pertsin, A.; Grunze, M.; Steitz, R.; Shchreiber, F. Interaction of Water with Self-Assembled Monolayers: Neutron Reflectivity Measurements of the Water Density in the Interface Region. *Langmuir* **2003**, *19*, 2284−2293.
(86) Pawlowska, N. M.; Fritzsche, H.; Blaszykowski, C.; Sheikh, S.; Vezvaie, M.; Thompson, M. Probing the Hydration of Ultrathin Antifouling Organosilane Adlayers Using Neutron Reflectometry. *Langmuir* **2014**, *30*, 1199−1203.
(87) Skoda, M. W. A.; Jacobs, R. M. J.; Willis, J.; Schreiber, F. Hydration of Oligo(Ethylene Glycol) Self-Assembled Monolayers Studied Using Polarization Modulation Infrared Spectroscopy. *Langmuir* **2007**, *23*, 970−974.
(88) Lane, J. M. D.; Chandross, M.; Lorenz, C. D.; Stevens, M. J.; Grest, G. S. Water Penetration of Damaged Self-Assembled Monolayers. *Langmuir* **2008**, *24*, 5734−5739.
(89) Tyrode, E.; Liljeblad, J. F. D. Water Structure Next to Ordered and Disordered Hydrophobic Silane Monolayers: A Vibrational Sum Frequency Spectroscopy Study. *J. Phys. Chem. C* **2013**, *117*, 1780−1790.
(90) Vericat, C.; Vela, M. E.; Salvarezza, R. C. Self-assembled monolayers of alkanethiols on Au(111): surface structures, defects and dynamics. *Phys. Chem. Chem. Phys.* **2005**, *7*, 3258−3268.
(91) Poirier, G. E. Mechanism of Formation of Au Vacancy Islands in Alkanethiol Monolayers on Au(111). *Langmuir* **1997**, *13*, 2019−2026.
(92) Poirier, G. E. Characterization of Organosulfur Molecular Monolayers on Au(111) Using Scanning Tunneling Microscopy. *Chem. Rev.* **1997**, *97*, 1117−1128.
(93) Sun, L.; Crooks, R. M.; Sun, L.; Crooks, R. M. Indirect Visualization of Defect Structures Contained within Self-Assembled Organomercaptan Monolayers: Combined Use of Electrochemistry and Scanning Tunneling Microscopy. *Langmuir* **1993**, *9*, 1951−1954.
(94) O'Dwyer, C.; Gay, G.; Viaris de Lesegno, B.; Weiner, J. The Nature of Alkanethiol Self-Assembled Monolayer Adsorption on Sputtered Gold Substrates. *Langmuir* **2004**, *20*, 8172−8182.
(95) Hu, Q.; Laskin, J. Secondary Structures of Ubiquitin Ions Soft-Landed onto Self-Assembled Monolayer Surfaces. *J. Phys. Chem. B* **2016**, *120*, 4927−4936.

DOI: 10.1021/acs.langmuir.9b00541
Langmuir XXXX, XXX, XXX−XXX